# FINAL PUBLISHABLE SUMMARY REPORT

**MODERN**
**(Contract No. 309314)**

**Modeling the Environmental and Human Health Effects of Nanoparticles**

**March 2016**

# Contents

# EXECUTIVE SUMMARY

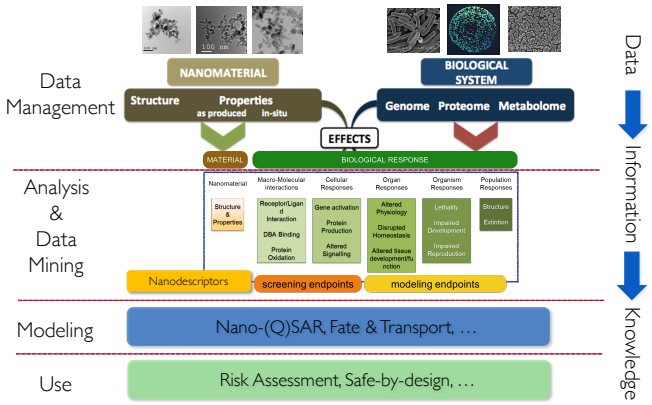


The aim of MODERN (Modeling the Environmental and Human Health Effects of Nanomaterials) is to develop a robust framework suitable for evaluating the environmental and health impact of engineered nanoparticles (eNPs). The main challenges that have been addressed to achieve the above objective are: (i) the development of nanoparticle categories based on their physicochemical, structural and toxicological properties, including their environmental and human health impacts, and (ii) the development of computational approaches for nanostructure characterization (nanodescriptors) and *in silico* models to assess nanoparticle effects.

The main outcomes of MODERN can be summarized as:

- New methodologies and tools for the computation of descriptors for nanoparticles with the focus on metals and metal oxides
- Synthesis and characterization of a library of metal and metal oxide nanoparticles for model testing and safe-by-design hypothesis validation.
- A web-based nanosafety data management system compliant with the ISA-TAB-Nano format to facilitate data exchange.
- A collection of ecotoxicity data via targeted experiments using MODERN's nanoparticle library openly accessible from MODERN's nanoDMS.
- Structure-activity relationships for nanomaterials based on selected properties and ecotoxicological endpoints and development of nanoparticle signatures that integrate biological information at multiple levels.
- A data-driven framework and basic categorization criteria for the identification of nanoparticle categories.
- A hazard ranking scheme suitable to rank eNPs and their categories according to their potential environmental and human health impact.

Regarding impact, the novel nanodescriptors and the new and improved toxicity models developed in the project enable to bring the understanding of the nanoparticle world out from the scientific community and research facilities and closer to the general public. The improved understanding of the safety issues of nanomaterials should have a twofold impact. First, a more knowledgeable public will be less accepting to poor practices of material handling and safety by the producers. Also producers of various nanomaterials would have an improved understanding of both the beneficial characteristics of their potential products but also the hazards at workplace and requirements for material handling. Regulators would have new and improved tools for assessing the safety of nanomaterials. Last, but not least, a knowledgeable public would be less likely to fall for any mass campaigns, either for or against the use of nanomaterials without analyzing the benefits and risks related to the real exposure scenarios in each particular case.

In conclusion, the overall expected impact of MODERN is the progress in understanding and describing the properties of nanomaterials, at scientific, production, regulatory and general public levels.

# SUMMARY DESCRIPTION OF THE PROJECT CONTEXT AND MAIN OBJECTIVES

The overall objective of MODERN is to develop a robust framework suitable for evaluating the environmental and health impact of engineered nanoparticles (eNPs). The main challenges that are addressed to achieve the above objective are: (i) the development of nanoparticle categories based on their physicochemical, structural and toxicological properties, including their environmental and human health impacts, and (ii) the development of computational approaches for nanostructure characterization (nanodescriptors) and *in silico* models to assess nanoparticle effects. Accordingly, the specific objectives to attain MODERN's overall research goal are: (i) to build a well-characterized library of eNPs with a comprehensive description of their structural, molecular and physicochemical properties; (ii) to develop and validate *in silico* models of biological activity of eNPs in organisms and in the environment from *in vitro*/*in vivo* toxicity profiling data; and (iii) to define and implement a categorization and hazard ranking methodology for eNPs based on structural similarity principles and toxicological profiles.
The specific scientific objectives for the project were:

- Development of new methodologies for the computation of basic descriptors for nanoparticles with the focus on metals and metal oxides (WP1).
- Synthesis and characterization of a basic library of metal and metal oxide nanoparticles for model testing and safe-by-design hypothesis validation (WP1).
- Development of a nanosafety data management system including structure, physicochemical properties and toxicity profiles of nanoparticles (WP2).
- Data generation (via targeted experiments using MODERN's nanoparticle library) and collection (via data sharing agreements and manual literature data curation) to populate MODERN's nanosafety data repository (WP2).
- Development of QNPRs/QNARs based on selected properties and ecotoxicological endpoints and development of nanoparticle signatures integrating biological information at multiple levels (WP2).
- Establishment of a data mining framework and basic categorization criteria for the identification of nanoparticle categories (WP3).
- Development of a hazard ranking scheme suitable to rank eNPs and their categories according to their potential environmental and human health impact.

The above objectives have been complemented by a set of dissemination & exploitation actions (WP4) and project management activities (WP5):

- Development and periodic update of project's website and dissemination of MODERN activities via social network tools (Facebook and Twitter) (WP4).
- Implementation of tools useful for different stakeholders (WP4).
- Dissemination of project results via peer-reviewed publications and conference presentations (WP4).
- Collaboration and information sharing with ongoing NMP projects in the NMP.2012.1.3-2, with other EC projects and EC NanoSafety Cluster, the OECD working party on manufactured nanomaterials (WPMN), and the Communities of Reseach (CoR) of the US-EU Dialogue on nanoEHS (WP4).
- Raising awareness of the methodologies and results of the project within various stakeholders (industry, regulators, and academy) and educating new generation (seminars, presentations) at postgraduate and PhD level in this very interdisciplinary study area.

# MAIN S&T RESULTS/FOREGROUNDS

In what follows, we describe the work done during the 36 months of the project. Relevant project outcomes are reported for each individual RTD work package. Results are summarized in the context of each project's objective.

**Objective: Synthesis and characterization of a basic library of metal and metal oxide nanoparticles for model testing and safe-by-design hypothesis validation.**

Although the number of unique eNPs and their innovative performance and growing, new engineered eNPs with novel physicochemical properties are posing health challenges to the human and the environment. These could include potentially hazardous interactions and a pressing need is felt for a comprehensive understanding of their toxicological properties and safer design. In depth research is needed to acquire knowledge in nanomaterial properties and their influence in bioavailability, transport, fate, cellular uptake, and catalysis of injurious biological responses. Additionally, extensive experimental protocols are also necessary to tailor the bio-impact across a spectrum of *in-vitro* to *in-vivo* nano-bio interfaces. To this end, MODERN has developed a well-characterized library of 12 metal-based nanoparticles using Flame Spray Pyrolysis (FSP). The FSP is a versatile process which is extremely appealing due to properties such as the generation of particles with crystalline perfection and with very large specific surface area and porosity (>95%). Using this novel technique, 12 metal-based nanoparticles (ZnO, CuO, $Co_3O_4$, $Fe_3O_4$, $Mn_3O_4$, $TiO_2$, $Sb_2O_3$, $Al_2O_3$, $SiO_2$, MgO, $WO_3$, and metallic Pd) have been synthetized. For the synthesis of these eNPs, metal-organic precursors such as zinc napthenate, copper napthenate, cobalt napthenate, iron napthenate, manganese napthenate, titanium (IV) isopropoxide, antimony (III) isopropoxide, aluminium secondary butoxide, tetraorthosilicate (TEOS), magnesium napthenate and palladium acetylacetonate were dissolved in a highly combustible organic solvent such as xylene to dilute the precursor and keep the metal concentration to 0.5 M. In order to design materials using FSP for demonstrating safer-by-design strategies, several nanoparticles were synthesized adapting controlled precursor chemistry and solvent combinations. In general, each liquid precursor (having 0.5M by metal) was delivered to the nozzle tip by a syringe pump at a flow rate of 5 mL/min by atomising the precursor solution with dispersant $O_2$ at a flow rate of 5mL/min and maintaining a pressure drop of 1.5 bar at the nozzle tip. Combustion of the dispersed droplets is initiated by the co-delivery of $CH_4$ and $O_2$ (1.5 L/min, 3.2 L/min) to form a flame. The flame parameters described above result in primary particle sizes of approximately 10 nm. The resulting ultrafine nanoparticles are highly crystalline with specific surface area and primary particle sizes in the range of 53 to 289 $m^2/g$ and 8-13 nm, respectively reasonably agreeing with the crystallite sizes derived from Rietveld fittings of the XRD patterns. Primary particle sizes were also confirmed by TEM analysis. The TEM micrographs demonstrate the particle shapes as well as their tendency to aggregate under dry conditions. After synthesis, the nanoparticle library was fully characterized in terms of their physicochemical properties.

**Objective: Development of new methodologies for the computation of basic descriptors for nanoparticles with the focus on metals and metal oxides.**

The development of *in silico* toxicity models for nanoparticles is mainly hindered by two factors: lack of appropriate descriptors and scarcity of consistent experimental data. While the latter is largely caused by the difficulties in synthesizing nanoparticles with well characterized and narrow size distribution, agglomeration, etc, the former is mainly caused by the very complex and large structures of nanoparticles (as compared to organic molecules) not permitting the use of most atom-explicit computational methods. MODERN has implemented two approaches for nanodescriptor development. The first is based on quantum chemistry calculations to describe the electronic structure of the nanoparticle whereas the second is based on molecular modeling principles.

**Development of Nanodescriptors based on nanoparticle's electronic structure.** Dimensionality has a significant impact on eNP reactivity. One of the presumable reasons why certain nanoparticles are found to be toxic is the fact that they catalyze certain reactions on their surface, and thus may generate toxic compounds. As most reactions catalyzed by metal oxide surfaces involve transfer of electrons in some stages (*i.e.*, redox reactions), knowledge of the electronic structure at the surface of the nanoparticle is pertinent. Four different types of rutile ($TiO_2$) systems (Figure 1) are shown to illustrate the approach used in MODERN to investigate these properties.

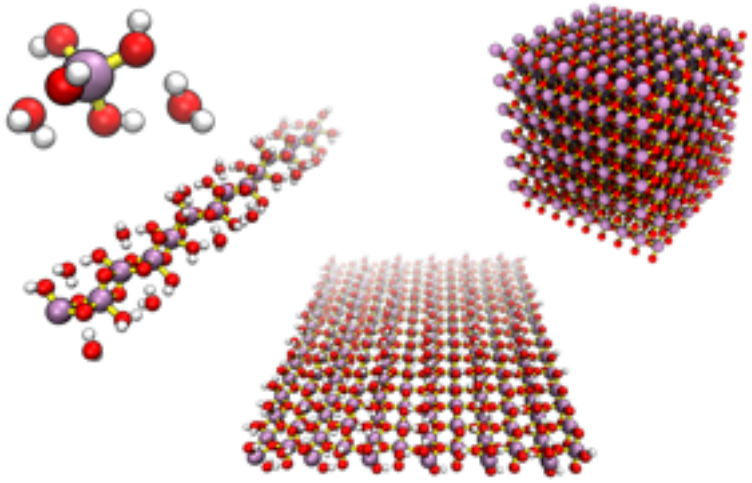

**Figure 1.** Four rutile ($TiO_2$) systems with different dimensionalities: Monomer (upper left), 1D-periodic rod (below), 2D-periodic layer (middle), 3D-periodic bulk phase (upper right).

Nanoparticles typically contain millions of atoms, and are therefore considered to be very large from the viewpoint of electronic structure theory. They no longer possess discrete electronic orbitals, but these orbitals are fused to form energy bands, as is well known from investigations of metals and semiconductors. A simple way to visualize such a band structure is a density of states (DOS) plot. In **Figure 2**, such a DOS plot is shown for plane wave (PW) calculations of rutile ($TiO_2$) in the following four dimensionalities: monomer (single molecule, approximated through a pseudo-isolated periodic slab approach), 1D-periodic (nanowire), 2D-periodic (nanosheet), and 3D-periodic (bulk crystal). For comparison, orbital energies of the highest four occupied and lowest four unoccupied electronic states of $TiO_2$ as truly non-periodic molecule are added as top row.

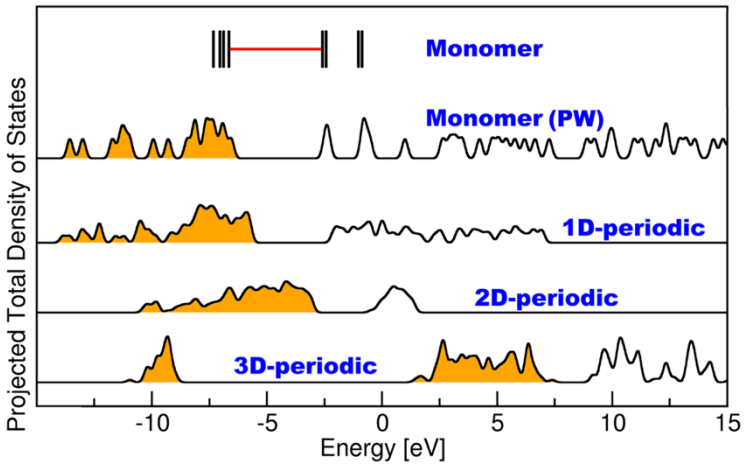


**Figure 2.** Density of states (DOS) vs. electronic state energy for rutile ($TiO_2$) in four dimensionalities, augmented by the orbital energies of $TiO_2$ as truly isolated non-periodic molecule.

In this figure, the density of available electronic states (Y axis) is plotted against the electronic state energy (X axis). The orange colour below the curves indicates up to which energy the states are occupied by electrons in the investigated material (Fermi level). All four systems possess an electronic band gap, meaning that occupied states do not directly merge into unoccupied states, but that there is a region with no electronic states at all that separates the valence band from the conduction band. Note further that the HOMO-LUMO energy difference (*i.e.*, the energy difference between highest occupied molecular orbital and lowest unoccupied molecular orbital) of $TiO_2$ as truly isolated compound ("Monomer" in **Fig. 1**) is very similar to the mean of the HOMO-LUMO band gap difference of its pseudo-isolated periodic-slab counterpart.
When switching on the intermolecular interactions in one, two or (all) three dimensions as addressed through periodic-slab calculations with respectively selected vacuum spacers in the unit cell, the HOMO-LUMO band gap becomes increasingly smaller. In **Figure 2**, this trend is seen when increasing the dimensionality through going from the PW-approximated monomer over the 1D-periodic and 2D-periodic to the 3D-periodic (bulk) system. The width of this band gap is an indicator for the ability of the material to accept and donate electrons to adsorbed species, and therefore is related to the catalytic activity at the surface. Accordingly, increasing the dimensionality makes the band gap increasingly narrow, implying a corresponding decrease in electronic hardness and thus an increase in reactivity.

**Effect of doping and impurities.** Another relevant outcome of MODERN concerns the influence of doping or other impurities on the electronic structure of metal oxide NPs. To capture this effect, the bulk phase rutile system shown in **Figure 1** was modified in several ways. Specifically, one titanium (Ti, ground-state valence-shell electron configuration $3d^2\ 4s^2$) atom was replaced by zirconium (Zr, $4d^2\ 5s^2$), scandium (Sc, $3d^1\ 4s^2$), vanadium (V, $3d^3\ 4s^2$), and a vacancy (*i.e.*, no atom at all), respectively. For these modified systems, the electronic structure was calculated both with and without allowing the geometry to relax after the replacement. The results are presented in **Figure 3**. It can be seen that replacing Ti by the isoelectronic Zr has almost no effect on the electronic structure and the band gap. If, however, one Ti atom is replaced by Sc (one less valence-shell electron), V (one more valence-shell electron) or a void, the orbital pattern is heavily affected, and the electronic band gap becomes much smaller. In case of Sc, there exists a partially occupied orbital exactly at the Fermi level, which corresponds to a completely vanishing band gap: A small amount of electron density can be either donated or accepted without any change in energy, leading to a very high redox activity. These electronic structure results thus demonstrate that doping as well as voids may be crucial for their redox activity, keeping in mind that real nanoparticles are never completely pure regarding their chemical composition.

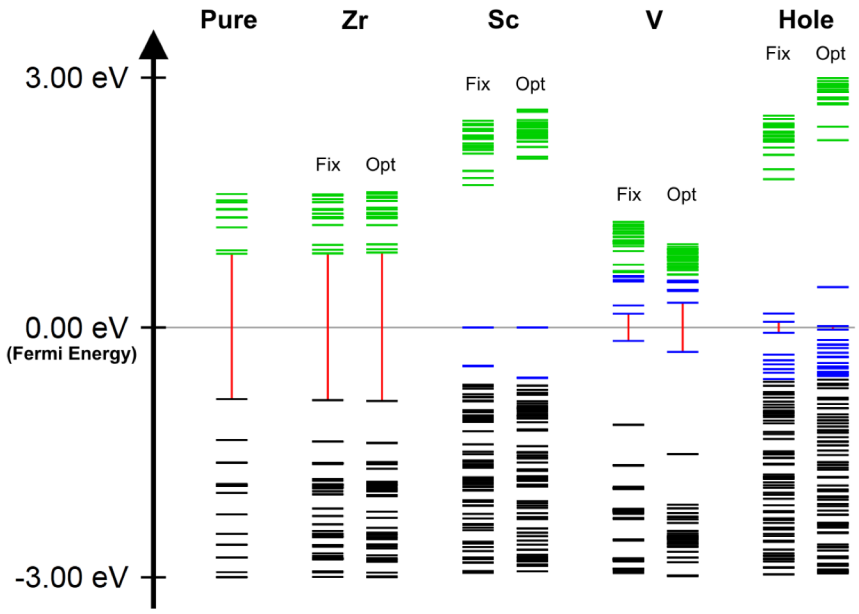


**Figure 3.** Influence of doping (one Ti atom of the unit cell replaced by Zr, Sc or V) and a void (hole = one Ti position in the unit cell empty) on the energy levels of bulk phase rutile ($TiO_2$). Fix = rutile geometry; Opt = geometry optimized with modified system. *Black:* occupied orbitals, *green:* unoccupied orbitals, *blue:* partially occupied orbitals.

Whereas these results have been calculated for the bulk phase as a 3D-periodic crystal, respective effects could be even more pronounced at the surface layer, and there add to the already present electronic perturbation caused by the fact that in contrast to bulk-phase lattice positions, surface-layer atoms are not surrounded by neighbouring solid-phase atoms and thus less shielded. Corresponding calculations, however, are computationally more demanding because an at least approximate atomic-level description of an NP surface layer would require an explicit inclusion of some additional layers below the surface in order to capture the electronic structure variation in the bulk-surface transition region. From this viewpoint, the 2D-periodic and 3D-periodic systems discussed above in the context of dimensionality (**Figure 2**) represent limiting cases of an isolated surface layer (that lacks any subjacent layers) and a perfect bulk phase (that lacks a surface layer), with a true surface layer being expected to show a somehow intermediate behaviour.

**Prediction of Infrared Spectra.** When it comes to identifying nanoparticle surfaces, infrared spectroscopy can be an important experimental tool. However, it is not always easy to assign bands in the spectrum to structural motifs of different surface types. By the use of ab initio molecular dynamics, infrared spectra of metal oxide surface slabs can be computed, which might be of aid for interpreting experimental results. **Figure 4** shows a computed infrared spectrum of a rutile 100 surface with and without adsorbed water molecules. As under ambient conditions always a certain amount of water is adsorbed to surfaces, the spectrum which includes the explicit solvation is assumed to be more realistic.

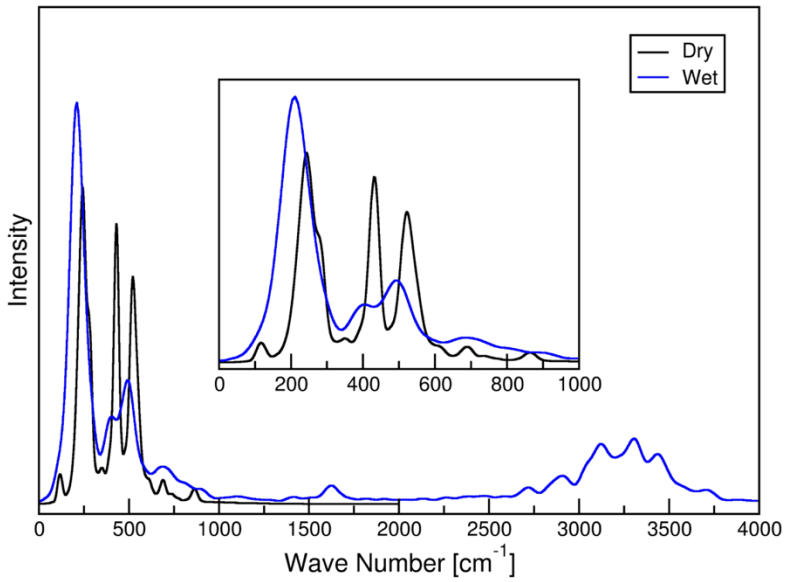


**Figure 4.** Predicted infrared spectra of rutile surface slab with (blue) and without (black) solvation by water.

**Development of size-dependent nanodescriptors.** One of MODERN's goals has been to find a solution to the lack of "true nanodescriptors" capable of distinguishing between the properties of compounds in the bulk and in nanoparticles of different sizes. To address this issue, the approach chosen was to model eNPs as whole-particles since it is the most consistent and size-aware option. Naturally, true quantum chemistry is not applicable to such large systems, therefore, molecular-mechanics/dynamics based methods have been used.
Using this approach, a series of descriptors derived from the full molecular mechanic simulation of metal oxide nanoparticles have been developed. Due to the increasing processing power of computers, it is possible to calculate the energy and structural parameters of nanoparticles in a relatively small timescale using simple interatomic potentials.

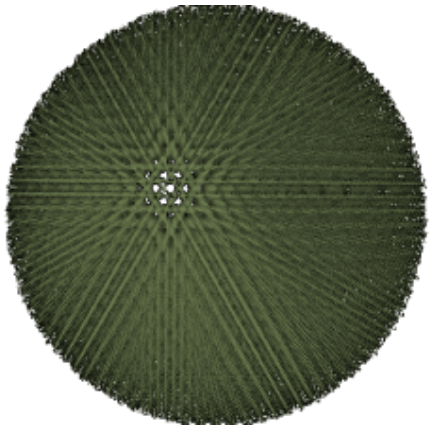

**Fig. 5** A sample of a spherical $SiO_2$ nanoparticle used for descriptor calculations at the force-field level. The size of the particle is 6.75 nm and it contains 102,579 atoms

The novel methodology developed in MODERN for nanodescriptor calculation comprises the following steps. First, atomic coordinates for the metal oxide nanoparticle are generated. The thermodynamically most stable crystal structure for each metal oxide is selected and the corresponding unit cell parameters are used to generate a spherical nanoparticle with the desired diameter (see **Fig. 5**). The atoms in this sphere are divided into two groups: core and shell. The atoms in the core are assumed to have similar characteristics to the bulk material while the shell

atoms are destabilized. While the positions of the atoms can be optimized according to different schemes, the approach works even without optimization. Already from a single-point calculation, the potential energy and coordination numbers can be extracted. These values are the basis to derive different categories of descriptors for nanoparticles (**Table 1**). Constitutional descriptors, reflecting the chemical composition, can be as simple as the number of metal or oxygen atoms in the two respective nanoparticle regions. Topological (i.e., connectivity based) descriptors include the average coordination number of metal and oxygen atoms in the shell group and in the core group. Descriptors based on potential energy can either be derived solely from the nanoparticle (average potential energy of metal atoms in shell regions) or in comparison with bulk material (difference between the lattice energy of nanoparticle and bulk material). Some of the 35 descriptors developed were specific to metal oxide eNPs (i.e., use parameters related to oxygen atoms or metal atoms) but the concept can be adjusted to pure metal NPs or other types of particles in a straightforward manner.

**Table 1.** Classes of size-dependent nanodescriptors for metal oxide eNPs

| **Descriptor related to** | **Basis of descriptors** |
|---|---|
| Chemical composition | Total number of atoms in nanoparticle, in the core and shell regions. |
| Potential energy | Average potential energy of all atoms in nanoparticle, of metal atoms or oxygen atoms, in electron volts. |
| Lattice energy | Lattice energy of the whole nanoparticle, relative lattice energy (per diameter or per surface area or as compared to a perfect crystal) of the particle in electron volts. |
| Topology | Average coordination number of all atoms, metal atoms or oxygen atoms in the nanoparticle. |
| Size | Diameter, surface area and volume of the nanoparticle in Å, Å$^2$, Å$^3$, respectively. |

**Nanodescriptor calculation.** The calculation of nanodescriptors was performed with the LAMMPS[1] molecular dynamics simulator program using Buckingham potentials to calculate the energies. First, the energy of the unit cell was calculated and the optimal cutoff values for Coulombic interactions were calibrated and later used for nanoparticle calculations. Atomic coordinates of nanoparticle were found by replicating the selected unit cell and cutting out the desired shape of the nanoparticle (sphere in the present case). To ensure the charge neutrality of the nanoparticle, an appropriate number of metal or oxygen atoms were added at random lattice positions on the surface of the nanoparticle. After that, descriptors from classes described in **Table 1** were calculated from the results of a single-point energy calculation.

A large number of the descriptors are derived from the potential energy which is composed of two parts: pairwise energy calculated by the Buckingham potential (**eq 1**), and Coulombic interactions, which are calculated by Wolf summation:

$$E_B = A * e^{-r/\rho} - \frac{C}{r^6} \quad r < r_c, \qquad (1)$$

where $A$, $\rho$, $C$ are constants of the Buckingham potential; r is the interatomic distance; $r_c$ is the cut-off radius. Wolf summation was used as the computationally much more affordable alternative to the traditional Ewald summation. The required cut-off radiuses for the Wolf summation were derived from the modeling of respective infinite crystals by periodic calculation of small clusters of crystal unit cells.

[1] http://lammps.sandia.gov

One of the main requirements for these calculations are the constants for Buckingham potentials. For many metal oxides, these values can be found from the literature, but for example $Sb_2O_3$, these constants had to be derived. Density functional theory (i.e., DFT at the level of B3LYP/Def2-TZVDP) was used to calculate the interatomic potential parameters. The ability to derive the interatomic potential fully theoretically based on *ab-initio* calculations and the subsequent calculation of descriptors using these parameters constitutes a great advantage since the only experimental parameter required for the calculation of nanodescriptors is the determined structure of the unit cell. As many metal oxides can exist in multiple crystal structures, the thermodynamically most stable crystal structure under standard conditions was used for the calculation of nanodescriptors in all cases. As an example, **Table 2** summarizes the values of the 35 nanodescriptors calculated for two nanoparticles of $TiO_2$ and $Al_2O_3$ with diameters of 20 and 60 nm, respectively.

**Table 2.** Descriptor classes and representatives of descriptors with examples of nanoparticles of $TiO_2$ and $Al_2O_3$ of 20 nm and 60 nm, respectively.

| **Geometric:** | **$TiO_2$** | **$Al_2O_3$** |
|---|---|---|
| *Diameter [nm]* | 20 | 60 |
| *Surface area [$nm^2$]* | 1259 | 11317 |
| *Volume [$nm^3$]* | 4201 | 113210 |
| **Constitutional (atom counts):** | | |
| *Number of atoms in eNP* | 402483 | 6544700 |
| *Number of atoms in core region* | 293465 | 5911572 |
| *Number of atoms in shell region* | 109018 | 633128 |
| *Number of metal atoms* | 134161 | 2617880 |
| *Number of metal atoms in core region* | 97789 | 2364696 |
| *Number of metal atoms in shell region* | 36372 | 253184 |
| *Number of oxygen atoms* | 268322 | 3926820 |
| *Number of oxygen atoms in core region* | 195676 | 3546876 |
| *Number of oxygen atoms in shell region* | 72646 | 379944 |
| **Potential energy based descriptors:** | | |
| *Average potential energy of atoms [eV]* | -40.31 | -28.37 |
| *Average potential energy of atoms in core region[eV]* | -40.48 | -28.43 |
| *Average potential energy of atoms in shell region [eV]* | -39.88 | -27,79 |
| *Average potential energy of metal atoms [eV]* | -78.99 | -42.53 |
| *Average potential energy of metal atoms in core region [eV]* | -79.34 | -42.62 |
| *Average potential energy of metal atoms in shell region [eV]* | -78.03 | -41.66 |
| *Average potential energy of oxygen atoms [eV]* | -20.98 | -18.93 |
| *Average potential energy of oxygen atoms in core region [eV]* | -21.05 | -18.97 |
| *Average potential energy of oxygen atoms in shell region [eV]* | -20.77 | -18.55 |
| **Topologic:** | | |
| *Average coordination number of all atoms* | 3.94 | 2.39 |
| *Average coordination number of all atoms in core region* | 4.00 | 2.40 |
| *Average coordination number of all atoms in shell region* | 3.78 | 2.26 |
| *Average coordination number of all metal atoms* | 5.91 | 2.98 |
| *Average coordination number of all metal atoms in core region* | 6 | 3 |

| | | |
|---|---|---|
| *Average coordination number of all metal atoms in shell region* | 5.67 | 2.83 |
| *Average coordination number of all oxygen atoms* | 2.96 | 1.99 |
| *Average coordination number of all oxygen atoms in core region* | 3 | 2 |
| *Average coordination number of all oxygen atoms in shell region* | 2.84 | 1.89 |
| **Lattice energy based descriptors:** | | |
| *Lattice energy [eV]* | -120.94 | -141.86 |
| *Difference between lattice energies of eNP and perfect crystal [eV]* | -0.50 | -0.31 |
| *Lattice energy divided by diameter of the eNP [eV/Å]* | -0.60 | -0.24 |
| *Lattice energy divided by surface area of the eNP [eV/Å$^2$]* | -9.60E-04 | -1.25E-04 |
| *Lattice energy divided by volume of the eNP [eV/Å$^3$]* | -2.88E-05 | -1.25E-06 |

Geometric descriptors are based on the calculated diameter of the nanoparticle, which is defined as the maximum distance between any two atoms in the nanoparticle. Constitutional descriptors are based on the chemical composition of nanoparticle. Descriptors which are based on the potential energy indicate the stability of the core and shell regions in the nanoparticle, respectively. Topologic descriptors are based on the coordination number of atoms (defined as counting the neighboring atoms which lie inside radius R.

$$R = 1.2 * (R_M + R_O) \qquad (2)$$

where $R_M$, $R_O$ are the ionic radii of metal and oxygen atoms, respectively. Finally, the last group of descriptors is based on the lattice energy, the difference of the latter compared to that of a perfect crystal and the proportion to diameter, surface area, and volume.

The main advantages of these nanodescriptors over previously published descriptors are:

1) Current descriptors require only one experimental parameter for calculation, namely the structure of the unit cell of the metal oxide. This information is available for many different metal oxides (and other compounds)
2) Descriptors are size-dependent.
3) Method for calculating descriptors is easily extendable to include solvent effects or to nanoparticles with non-spherical shape.

The unit cell structure is necessary to calculate the required constants for the Buckingham potential and to generate the structure of the nanoparticle. While at the moment the thermodynamically most stable crystal structure is used, in principle any other crystal structure can be used if so desired.

**Analysis of size-dependency.** Verifying the size-dependency of the new nanodescriptors is paramount, as the nanoparticles with the same chemical composition but different size can have different toxicity/property values. The size-dependency of a $Cr_2O_3$ nanoparticle descriptor *"Difference between lattice energies of nanoparticle and perfect crystal"* is depicted on **Figure 6**.

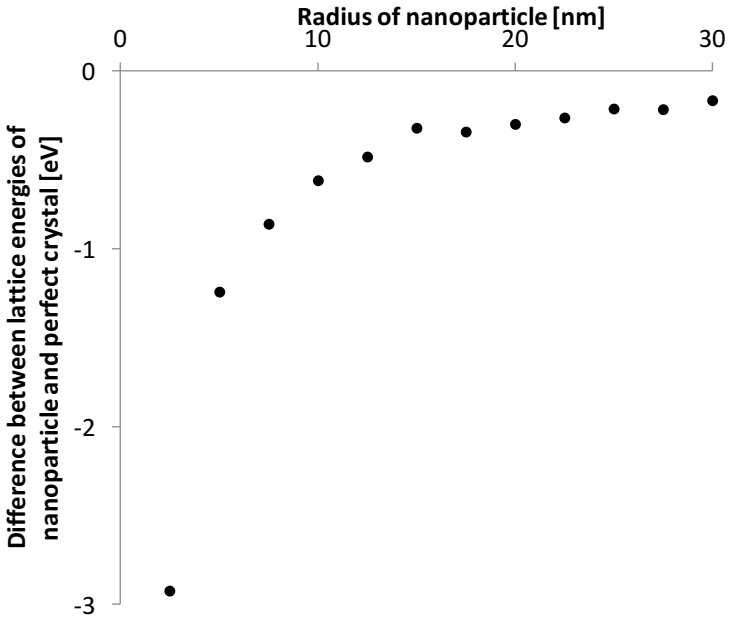


**Fig. 6** The size-dependency of the descriptor *"Difference between lattice energies of nanoparticle and perfect crystal"* for a $Cr_2O_3$ nanoparticle**.**

As the radius of nanoparticle increases, the difference between lattice energy of nanoparticle and the corresponding perfect crystal is reduced, approaching a constant. This follows the notion that as the size of nanoparticle approaches macroscopic levels, the properties of the nanoparticle start to become similar to the ones of macroscopic particle/bulk material. The curve presented in **Figure 8** agrees well with the commonly accepted position that nanoparticles of size below 20 nm require the most attention as they start to possess significantly different properties as compared to bulk material. A web-based application has been developed to obtain the values of the different nanodescriptor types for a set of 24 metal oxide nanoparticles. The application can be accessed from http://nano_descriptors.biocenit.cat and also provides interpolated estimations for any nanoparticle sizes in the range of 5 nm to 30 nm.

**Objective: Development of a nanosafety data management system including structure, physicochemical properties and toxicity profiles of nanoparticles (WP2).**

The development of reliable nanosafety assessment strategies requires the compilation of a significant amount of very heterogeneous data (e.g., emission sources, nanoscale properties, intermedia distribution, transformations and persistence, and effects in biological systems). Although these data are rapidly emerging, there is still a critical need for implementing efficient data management protocols aimed to facilitate data retrieval, transparent data sharing and the development of robust structure/property/activity relationships. To be effective, nanosafety data repositories must provide researchers and regulators with tools for knowledge extraction from annotated data. Data collected from nanotechnology research are fundamental for the identification of correlations between nanomaterial's structure, physicochemical properties and biological activity. Establishing these relationships is of paramount importance to identify mechanisms of toxicity and to guide safe-by-design strategies for new nanomaterials. Currently, most of the data on nanosafety are widely scattered and remain inaccessible as tables and figures in scientific literature or in non-public databases (e.g., research project results and industrial R&D activities). Data ambiguity, the lack of standardization together with unstructured and heterogeneous data sources makes the impact assessment of nanomaterials a challenging task plagued with uncertainties. The use of ontologies (i.e., controlled vocabularies and relationships

that capture knowledge in a specific domain) provides a unifying approach for data structuring and annotation. The use of standards for data annotation allows the integration of heterogeneous data sources, aggregation and presentation in an accessible format and facilitates the computational analysis of the integrated data sets.

To extract the maximum amount of relevant information, nanomaterial data should not be analysed independently of the overall nanosafety context. For instance, data only on *in vitro* toxicity effects are not sufficiently relevant/informative to get the complete picture of the potential impact of a nanomaterial. Additional information such as *in situ* nanomaterial properties, information on synthesis process, exposure conditions and actual dose and distribution of the particles taken up by cells/animals, and characteristics of the biological endpoint are also required. Based on these principles, a data management system with full support for ontology annotation was conceived and implemented in MODERN. The function of the data management system is to store nanosafety data in a semantically consistent manner by leveraging existing ontologies for specific parts of the nanosafety domain. In addition, the system has been designed to be interoperable and to facilitate data sharing. To this end, the data management system implements the ISA-TAB-Nano data exchange format.

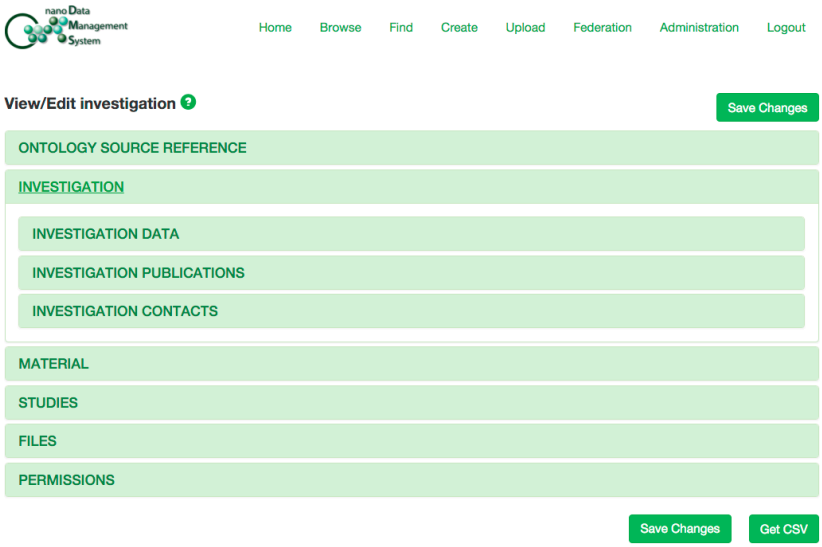


**Figure 7.** Web interface of the nanoDMS system showing the ISA-TAB_Nano structure**.**

The *nano Data Management System*[2] (nanoDMS, see **Figure 7**) developed in MODERN is available from the project website in different formats including source code, pre-pacakged binaries or virtual machines based on docker containers. Within MODERN, the use of the data management system has been complemented by the development of procedures for the curation of data so that data quality and provenance information are ensured. The usability of the system has been evaluated in collaboration with other modelling projects (e.g., nanoPUZZLES[3], Marchese Robinson et al., 2015). The system provides different access control levels to protect data confidentiality, integrity and preserve intellectual property rights. The system developed in MODERN also offers support for server federation, allowing the easy deployment of a distributed nanosafety cloud.

**Objective: Data generation (via targeted experiments using MODERN's nanoparticle library) and collection (via data sharing agreements and manual literature data curation) to populate MODERN's nanosafety data repository.**

In the context of experimental data generation, MODERN has contributed to advance the science of nanosafety in the following two areas. First, in the analysis of published nanotoxicity. Second,

[2] http://nanodms.biocenit.cat

[3] http://www.nanopuzzles.eu/

in the generation (and analysis) of toxicity data by targeted experiments with bacteria, protozoa and algae, using MODERN's nanoparticle library.

**Analysis of published literature data.** Data on some of the most widely used antimicrobial eNPs, such as ZnO, CuO and Ag eNP were collected from the published literature, analyzed and summarized (Bondarenko et al. 2013). The toxicity of these particles to algae, crustaceans, fish, bacteria, yeast, nematodes, protozoa and mammalian cells was compared to that of soluble salts of Zn, Cu and Ag.

Despite varying test methods and inconsistencies in particle characterization some trends in the toxicity data could be observed. For example, it was found that the toxicity values of CuO and ZnO NPs to mammalian and bacterial cells, varied in a relatively narrow range: 16-fold and 20-fold for ZnO NPs and 8-fold and 14-fold for CuO eNPs, compared to the toxicity values of Ag NPs varied 275-fold for mammalian cells *in vitro* and 500-fold for bacteria (**Fig. 8**). This difference can be attributed to nanoparticle coating: while the ZnO and CuO NPs were all uncoated, most of the studied Ag eNPs had various coatings (PVP, peptide, mono- and disaccharides etc.). It also appeared that the uncoated Ag eNPs were remarkably less inhibitory to bacteria than coated NPs. Nanoparticle coating was thus identified as a crucial element of safety analysis.

The relationship between particle size and toxicity was found only when comparing values presented in a single paper, or even using a single endpoint in a single paper. For example, when plotting all the toxicity values of PVP-coated Ag eNPs to mammalian cells against particle size, no correlation was observed ($r^2$ = 0.1), however, when using data from just one paper the correlation became evident ($r^2$ = 0.4) and improved further with the selection of just one cell line ($r^2$ = 0.8). Similar observations for other particles/test systems indicate inter-laboratory variations in preparation of eNP suspensions and testing conditions that complicate data comparison.

It was found that the toxicity of ZnO eNPs and Zn ions to different organisms was similar; indicating that the toxicity of ZnO eNPs can be explained by dissolved Zn. As illustrated in **Figure 8**, the L(E)$C_{50}$ values of Ag and ZnO eNPs correlated well with the respective values of the soluble salts ($r^2$=0.84 and 0.85, respectively), whereas the plot of CuO NPs and Cu ions formed two clusters, distinguishing mammalian cells, yeast and bacterial cells from all other organisms.

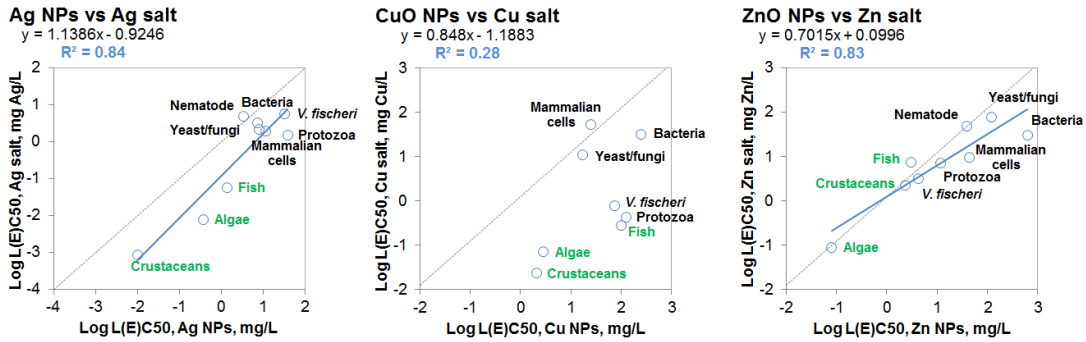


**Figure 8.** Plots of the median L(E)$C_{50}$ values of Ag, CuO and ZnO NPs *versus* the median L(E)$C_{50}$ values of the respective soluble metal salts to different organism groups, from Bondarenko et al. (2013).

A further literature review of Ag, ZnO and CuO toxicity was compiled with a focus on toxicity mechanisms (Ivask et al. 2014a). For that, 167 publications related to (eco)toxicology and mechanism of action of Ag NPs, ZnO NPs and CuO NPs were analyzed. Three major phenomena were found to drive the toxicity of the selected nanoparticles: a) dissolution of nanoparticles, b) organism dependent cellular uptake and c) induction of oxidative stress and consequent cellular damage. It was noticed that the published studies exploring Quantitative Nanostructure-Activity Relationships rely on a few and tailor-made experimental datasets.

**MODERN's targeted experiments.** The set of 12 eNPs in MODERN's library (ZnO, CuO, TiO2, Fe3O4, Co3O4, Mn3O4, SiO2, Al2O3, WO3, Sb2O3, MgO and Pd) were used for model

development and safe-by-design hypothesis testing based on previously published toxicity and solubility data. The particles, synthesized using FSP, were characterized in terms of their physicochemical properties by X-ray diffraction, Brunauer–Emmett–Teller (BET) analysis and TEM imaging (Ivask et al. 2015). In addition, bioactivity characterization was performed and included the following acute toxicity assays:

1) *Vibrio fischeri* kinetic bioluminescence inhibition assay (a Flash-test);
2) Bacterial and algal viability assay 'spot-test' using *Staphylococcus aureus* RN4220, *Escherichia coli* MG1655 and the alga *Pseudokirchneriella subcapitata*
3) Cell viability assay with the protozoan *Tetrahymena thermophila*
4) Algal growth inhibition assay with *P. subcapitata*

$EC_{50}$ values were calculated from the continuous toxicity data obtained from the above assays (**Figure 9**). The algal growth inhibition test was clearly the most sensitive assay, yielding $EC_{50}$ values for 10 out of the 12 NPs, whereas only 4 and 5 NPs showed significant toxicity to the protozoan and bacterium respectively.

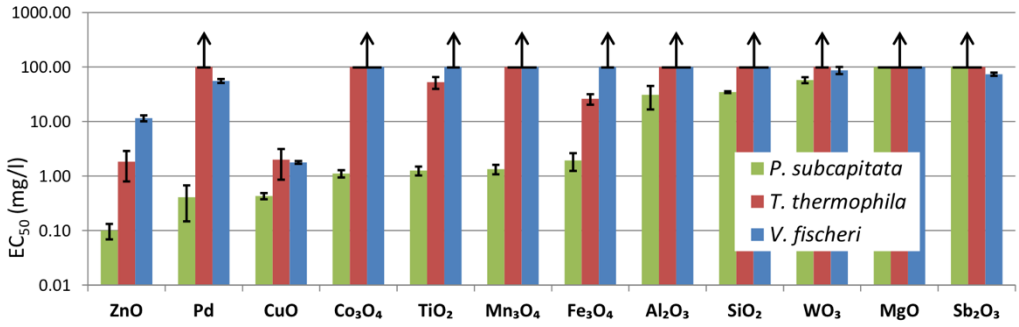


**Figure 9.** Toxicity of 12 nanoparticles to alga *Pseudokirchneriella subcapitata*, protozoan *Tetrahymena thermophila* and bacterium *Vibrio fischeri*. Arrows indicate EC50 values above 100 mg/l. From Aruoja et al. (2015)

Experimentally determined $EC_{50}$ values based on *P. subcapitata* growth inhibition values ranged from 0.10 mg/l for ZnO and 0.43 mg/l for CuO to 57.8 mg/l ($WO_3$), spanning three orders of magnitude. Only MgO and $Sb_2O_3$ were not toxic to algae ($EC_{50}$ >100 mg/l). Besides the effects of soluble ions of zinc and copper, the most significant mechanism of algal toxicity was co-agglomeration of NPs and cells that physically isolated the alga from nutrients/light energy. The formation of agglomerates that contained algal cells and NPs was observed for most of the studied NPs, only excluding ZnO, $WO_3$, $SiO_2$ and $Sb_2O_3$. However, based on the results of the viability assay it is likely that the cells inside the agglomerates were alive. For example, the $EC_{50}$ of Pd in the growth inhibition test was 0.4 mg/l, whereas the minimal biocidal value (24 h MBC) in DI water based on the 'spot' assay was 10 mg/l. Nevertheless, algal growth inhibition assay has proven far more sensitive than the 'spot' assay also for "conventional" soluble chemicals that do not entrap algae, such as $AgNO_3$: the 24 h MBC (in DI water) was 10 mg $AgNO_3$/l (Suppi et al. 2015) whereas the 72 h $EC_{50}$ in the growth inhibition assay was 0.007 mg Ag/l. (Ivask et al. 2014b) The algal toxicity mechanisms were studied in detail, revealing solubilisation as a probable cause of ZnO toxicity, whereas formation of ROS in abiotic conditions correlated with the toxicity of other NPs in the library (see Aruoja et al. 2015 for details).

In addition, the bacterial and algal cells were incubated with NPs in deionized water for 24h and then plated on agar media in order to determine the minimal biocidal concentrations. This eliminated the effects related to the interaction of NPs with components of test media (Suppi et al. 2015). Results obtained this way show relatively less toxicity compared to other assays used (**Table 3**).

**Table 3.** The minimal biocidal concentrations (MBC) of 12 metal containing nanoparticles to bacteria *Escherichia coli* , *Staphylococcus aureus* and alga *Pseudokirchneriella subcapitata*. The presented toxicity values are based on nominal exposure concentrations used in testing.

| NP | 24h MBC[a] E. coli (Gram -) | 24h MBC[a] S. aureus (Gram +) | 24h MBC[a] P. subcapitata |
|---|---|---|---|
| | mg compound/l | | |
| ZnO | 10 | 10 | 100 |
| Pd | 10 | 100 | 10 |
| CuO | 1 | 0.1 | 100 |
| Co3O4 | 100 | >100 | >100 |
| TiO2 | >100 | >100 | >100 |
| Mn3O4 | >100 | 100 | >100 |
| Fe3O4 | 100 | 100 | >100 |
| Al2O3 | >100 | >100 | >100 |
| SiO2 | >100 | >100 | >100 |
| WO3 | >100 | >100 | >100 |
| Sb2O3 | >100 | >100 | >100 |
| MgO | >100 | >100 | >100 |

a - The lowest tested conentrations that completely inhibited visible growth on the agarized test medium at 25°C after 24h of incubtion.

The absence of buffer in the test medium may cause pH-related effects on toxicity values. However, this did not appear to be the case since neither the sample with the lowest nor the highest pH (Sb2O3, pH=4.2 and MgO, pH=9.6, respectively) inhibited bacterial/algal growth. Among the 12 tested NPs in MODERN the greatest antibacterial activity was shown for CuO, ZnO and Pd (**Table 3**).

In order to compare the toxic effects of the studied 12 NPs to different test species, NPs were grouped according to assay type and $EC_{50}$ values (**Table 4**). Despite different species and test formats there were common features in terms of toxic effects. CuO and ZnO were the most toxic NPs to all the species regardless of the assay and endpoint. Also Pd was toxic to alga and bacteria *E. coli* at relatively low concentration (<10 mg/l) and $Co_3O_4$ showed toxic effects to the alga (<10 mg/l) and *E. coli* (<100 mg/l). MgO was the only NP that was not toxic to any test organism in any test setting (i.e. $EC_{50}$ or MBC > 100 mg/l), in addition to MgO, for the majority of test species and test settings $Al_2O_3$, $Co_3O_4$, $Fe_3O_4$, $Mn_3O_4$, $SiO_2$, $TiO_2$ showed no toxic effects below 100 mg/l. The most sensitive test was algal growth inhibition assay according to which only MgO and $Sb_2O_3$ proved not toxic even at 100 mg/l and CuO, ZnO and Pd showed growth inhibitory effects at very low concentrations (< 1 mg/l).

**Table 4** Categorization of NPs based on the toxicity values ($EC_{50}$ or MBC, mg compound/l) to bacteria, protozoa and algae. All NPs were tested in nominal concentrations from 0.01 up to 100 mg/l.

| $EC_{50}$ or MBC, mg compound/l | **72 h $EC_{50}$** | **24 h $EC_{50}$** | **30 min $EC_{50}$** | **24 h MBC** | **24 h MBC** |
|---|---|---|---|---|---|
| Organisms: | Algae | Protozoa | Bacteria | Bacteria | Bacteria |

| Species: | *Pseudokirchneriella subcapitata* | *Tetrahymena thermophila* | *Vibrio fischeri* (*G*-) | *Escherichia coli* (*G*-) | *Staphylococcus aureus* (*G*+) |
|---|---|---|---|---|---|
| Exposure medium: | Mineral medium | DI water | 2 % NaCl | DI water | DI water |
| **0.1-1** | **CuO, ZnO, Pd** | **None** | **None** | **CuO** | **CuO** |
| **>1-10** | **$Co_3O_4$, $Fe_3O_4$, $Mn_3O_4$, $TiO_2$** | **CuO, ZnO** | **CuO** | **ZnO, Pd** | **ZnO** |
| **>10-100** | **$Al_2O_3$, $SiO_2$, $WO_3$** | **$Fe_3O_4$, $TiO_2$** | **ZnO, Pd, $WO_3$, $Sb_2O_3$** | **$Co_3O_4$, $Fe_3O_4$** | **$Fe_3O_4$, $Mn_3O_4$, Pd** |
| **>100** | **MgO, $Sb_2O_3$** | **$Al_2O_3$, $Co_3O_4$, MgO, $Mn_3O_4$, Pd, $Sb_2O_3$, $SiO_2$, $WO_3$** | **$Al_2O_3$, $Co_3O_4$, $Fe_3O_4$, MgO, $Mn_3O_4$, $SiO_2$, $TiO_2$** | **$Al_2O_3$, MgO, $Mn_3O_4$, $Sb_2O_3$, $SiO_2$, $TiO_2$, $WO_3$** | **$Al_2O_3$, $Co_3O_4$, MgO, $Sb_2O_3$, $SiO_2$, $TiO_2$, $WO_3$** |

**Objective: Development of QNPRs/QNARs based on selected properties and ecotoxicological endpoints and development of nanoparticle signatures integrating biological information at multiple levels.**

The main reason for developing novel nano-descriptors in the framework of MODERN was the fact that while several previous Quantitative Structure-Activity/Property Relationships had been developed considering the properties of nanoparticles, these nano-QSARs (QNARs) relied typically just on the chemical composition of the nanoparticles rather than considering (also) the single most characteristic feature of nanoparticles – their size. Indeed, prior to the launch of MODERN, no QNAR took into account the size or shape of nanoparticles. Such models can only perform meaningfully under certain conditions (e.g., no size distribution in dataset, very limited or inconsistent experimental data leading to noisy unstable models and perhaps overfitting) and cannot, thus, be considered as true QNARs.

**Identification of structure-activity relationships from nanoparticle's electronic structure descriptors.** In recent years it became apparent that besides the often-discussed redox activity of nanoparticles that may induce reactive oxygen species (ROS), other toxicological pathways may play a role. In this context, a particular issue is phagocytosis (Trojan horse) as highly efficient route of uptake into the cell, offering the possibility of metal-specific toxicity at very high concentrations upon intracellular dissolution. In the following, MODERN generated algal toxicity data in terms of 72-h $EC_{50}$ (i.e., growth inhibition 50%) values were analyzed from the viewpoint of quantum chemical reactivity parameters calculated for eNP monomers, including trend analyses of the electronic structure characteristics when going from the monomers to clusters with increasing molecular size.

Algal toxicity data in terms of 72-h $EC_{50}$ [mg/L] values -effective concentration inhibiting the growth by 50%- for a subset of metal oxide nanoparticles ($Al_2O_3$, CuO, $Fe_2O_3$, MgO, $Sb_2O_3$, $SiO_2$, $TiO_2$ and ZnO) were used as endpoint. For their conversion from the original mass-based unit to mol/L, the molar mass of the respective unit cell was divided by its number of metal atoms, considering the fact that in this way, the toxicity is normalized to the concentration of metal ions. Taking the $Al_2O_3$ NP as an example, the crystal monomer is $Al_2O_3$, yielding $AlO_{1.5}$ as formal basis for the NP molar mass. The resultant log $EC_{50}$ [mol/L] values were used for comparison with electronic structure characteristics.

The starting geometries for the metal oxide clusters were prepared in the following way. For each cluster, a part was cut out of the solid-state crystal structure of the material, such that the number of metal atoms (which were used as a measure for the cluster size) was as desired. The cutting was performed in such a way that the surface of the resulting cluster is completely terminated with oxygen atoms. Subsequently, hydrogen atoms have been added to exposed oxygen atoms in order to obtain a neutral charge, turning some oxygen atoms into hydroxyl groups and others into water molecules. This creates a microsolvation around the cluster, and keeps the coordination

number of the metal atoms at the same value as in the bulk phase. To give an example, the cluster containing one aluminum atom was cut out of the corundum lattice as formal "$AlO_6$", because aluminum has six nearest oxygen neighbors in the lattice. Subsequently, hydrogen atoms were added, turning three of the oxygen atoms into hydroxyl groups and the remaining three into water molecules, thus yielding a final cluster of $Al(OH)_3(H_2O)_3$ that is neutral in charge.
The quantum chemical calculations were performed with the program package Orca, employing density functional theory (DFT) with the PBE functional and Grimme's empirical D3 dispersion correction. Atom-centered basis sets of the type def2-TZVPP were used for all atoms. The SCF convergence criterion was set to *"VeryTight"*. The starting structures of all metal oxides (i.e., monomers and clusters containing an increasing number of monomer units) have been cut from the corresponding solid state lattices, and subsequently the exposed surfaces have been saturated by hydroxide ions to obtain charge-neutral species. Water molecules were added to account for solvation effects ("microsolvation"). Based on these structures, geometry optimizations (convergence criterion "Tight") was performed to determine equilibrium geometries. IP, EA, $\varepsilon_F$ (–EN) and HD as electronic structure characteristics have been calculated from the respective DFT orbital energies based on Koopmans.

**Trend analysis.** The data distributions of log $EC_{50}$ [mol/L] of the eight eNPs vs. calculated IP, EA, $\varepsilon_F$ (= –EN) and HD of the NP monomers (saturated by H atoms) are shown in **Figure 10**. As can be seen from the top left plot, NP toxicity vs. IP suggests a separation between the main-group metal oxides MgO, $Sb_2O_3$, $SiO_2$ and $Al_2O_3$ on the one hand, and the transition-metal oxides CuO, ZnO, $Fe_2O_3$ and $TiO_2$ on the other hand.

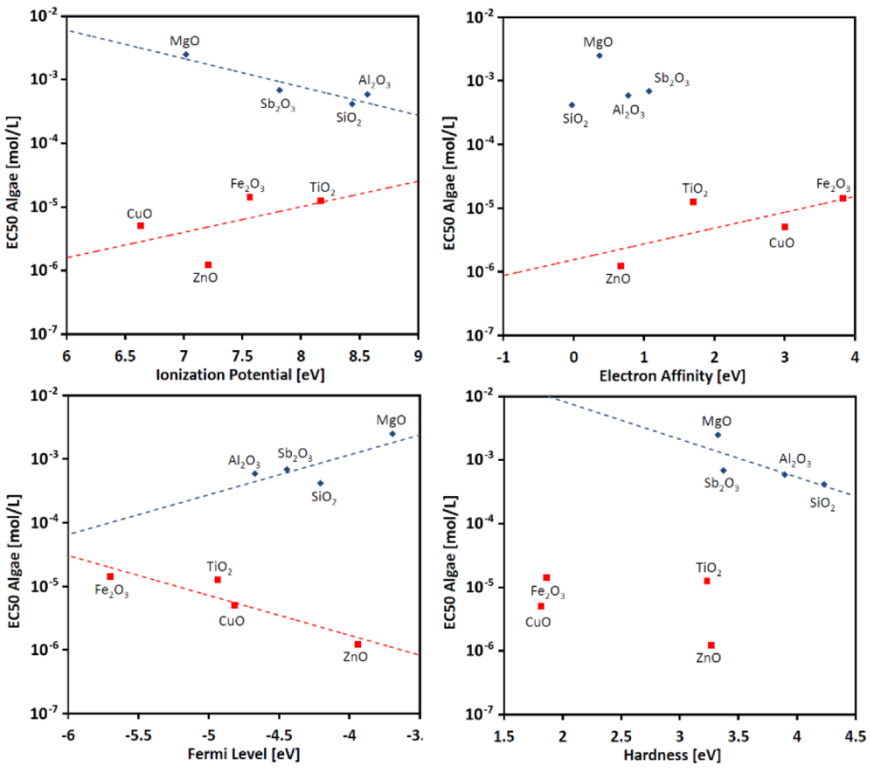


**Fig. 10** Algal toxicity in terms of logarithmic-scale 72-h $EC_{50}$ of eight NP metal oxides vs. calculated ionization potential (IP, top left), electron affinity (EA, top right), Fermi level ($\varepsilon_F$, bottom left) and hardness (HD, bottom right) from the DFT HOMO and LUMO energies employing Koopmans theorem.

Whereas both subsets overlap in their IPs as estimated through Koopmans theorem from the HOMO energies, the high toxicity end of the former (log $EC_{50}$: from –2.6 for MgO to –3.4 for $SiO_2$) differs by 1.5 log units from the low toxicity end of the latter (log $EC_{50}$: from –4.9 for $Fe_2O_3$

to –5.9 for ZnO). Moreover, eNP toxicity increases with decreasing IP for the transition-metal eNPs, which contrasts with the opposite trend observed for the main-group counterparts. Since the IP is inversely related to the ease of electron donation, the latter appears to play a toxicity-enhancing role only for algal toxicity of the transition-metal oxide eNPs, suggesting a redox-mediated toxicity pathway in contrast to a different toxicological mode of action for the main-group oxide NPs.

In the top right plot of **Figure 10**, a similar discrimination between the main-group and transition-element metal oxide eNPs is shown with EA as eNP monomer property. In this case, increasing EA corresponds to an increase in algal toxicity for the transition metals, indicating that the latter is enhanced with increasing capability of accepting excess electronic charge. Regarding the Fermi level of the eNP monomers (bottom left in **Figure 10**), eNP toxicity increases with increasing $\varepsilon_F$, suggesting that the NP electron donor strength provides a significant contribution to the algal toxicity. The corresponding decrease in toxicity with increasing EN (= $-\varepsilon_F$) is in line with this interpretation and indicates that in contrast to the main-group metal oxides, the transition-metal eNPs show a decrease in toxicity with increasing initial electron attraction.

When analyzing log $EC_{50}$ from the viewpoint of the electronic hardness (that is inversely related to the polarizability), a similar between-group separation is accompanied by less pronounced within-group trends. In this case, the main-group metal oxides show a weak increase in toxicity with increasing HD, which would also hold with regard to ZnO as compared to the other three transition-metal oxides, but not otherwise. Taking all four plots of **Figure 10** together, the level of significant approximation regarding eNP electronic properties should be kept in mind, which concerns both fundamental and methodological issues (eNP monomer vs eNP bulk vs eNP surface, Koopmans theorem, DFT computational chemistry).

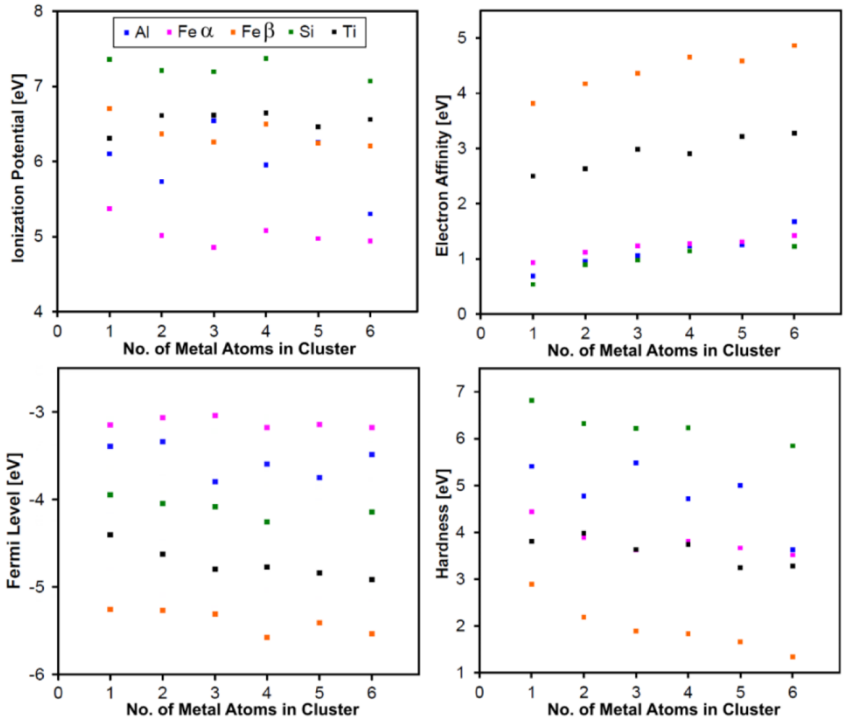


**Fig. 11** Dependence of electronic reactivity parameter (top left: IP; top right: EA; bottom left: $\varepsilon_F$; bottom right: HD) on cluster size of the metal oxide ($Al_2O_3$, $Fe_2O_3$, $SiO_2$, $TiO_2$) expressed through the number of metals ions included; Fe α and Fe β refer to the α and β spin orbital subsets (see text).

To explore the property trend when increasing the cluster size of the atomic-level description, respective calculations have been undertaken for $Al_2O_3$, $Fe_2O_3$ (α and β spin orbital subsets resulting from high-spin open-shell calculations), $SiO_2$ and $TiO_2$. The results are summarized in **Figure 11**, showing dependence of IP, EA, $\varepsilon_F$ and HD on cluster size in terms of its number of

monomer units (ranging from 1 to 6). For most properties and clusters, reasonably monotonic trends are seen, with notable exceptions for $Al_2O_3$ as well as for IP.
In summary, the above quantum chemical analysis of the algal toxicity of metal-oxide eNPs suggests a significant difference in mode of action between the subgroups of transition metals and main-group elements. For the former, toxicity increases with increasing electron-donor capability, indicating that a redox-mediated process involving electron transfer to reactive oxygen species (ROS) plays a crucial toxicological role. Alternatively, and considering the experimental setting with exposure to light and thus radiation energy, the increase in toxicity with decreasing IP may also reflect an increased probability for electronic transitions into the excited state and thus a phototoxic contribution to the observed algal growth inhibition in terms of 72-h $EC_{50}$ values. For the main-group elements, the lack of respective $EC_{50}$ dependencies suggests a non-ROS mode of toxic action.

**QNAR development from size-dependent nanodescriptors.** The principal novel concept in MODERN's size-dependent nanodescriptor approach relied on the variation of interatomic potential energies as a function of atom types and coordination, thus capturing both the role of chemical identity as well as that of surface to volume ratio. In order to verify the performance of the developed descriptors, QNARs were constructed. A sample data set for QNAR modeling was obtained from Pathakoti et. al.[4] containing *E. coli* $EC_{50}$ data of metal oxides, measured in the dark.

**Table 5.** Experimental and predicted $log(1/EC_{50})$ values of nanoparticles, calculated nanodescriptors (ND) and diameters.

| | $log(1/EC_{50})$ | | Nanodescriptors | | NP size |
|---|---|---|---|---|---|
| **NP** | **Exp.** | **Pred.** | **$D_3$(eV)** | **$D_4$(eV)** | **Diameter (nm)** |
| $Al_2O_3$ | 2.42 | 2.7 | -30.85 | -5.75 | 55 |
| $Bi_2O_3$ | 3.55 | 3.52 | -17.69 | -7.25 | 144 |
| CoO | 3.13 | 3.57 | -20.12 | -6.34 | 55 |
| $Cr_2O_3$ | 2.06 | 2.77 | -30.83 | -5.55 | 47 |
| CuO | 4.24 | 3.83 | -20.33 | -5.45 | 28 |
| $Fe_2O_3$ | 2.4 | 2.69 | -30 | -6.04 | 68 |
| $In_2O_3$ | 2.83 | 2.91 | -28.19 | -5.9 | 60 |
| $La_2O_3$ | 4.96 | 4.3 | -12.53 | -6.36 | 65 |
| NiO | 3.79 | 4.16 | -20.11 | -4.55 | 14 |
| $Sb_2O_3$ | 3.12 | 2.74 | -28.4 | -6.34 | 84 |
| $SiO_2$ | 2.54 | 1.97 | -42.44 | -4.52 | 20 |
| $SnO_2$ | 2.53 | 2.56 | -38.11 | -4.19 | 15 |
| ZnO | 5.8 | 5.77 | -19.64 | -2.10E-07 | 71 |
| $ZrO_2$ | 2.58 | 2.76 | -32.63 | -5.02 | 27 |
| $TiO_2$ | 2.14 | 1.84 | -40.87 | -5.5 | 42 |

The developed model had the following equation:

$$log(1/EC_{50}) = 7.69 + 0.10D_3 - 0.34D_4, \qquad (3)$$

where $D_3$ is the descriptor "Average potential energy of atoms in core region of nanoparticle" in eV, $D_4$ is the "Lattice energy of nanoparticle per unit volume" in eV/Å3, both given in electron volts. The statistical parameters of the model were found to be: squared correlation coefficient $R^2 = 0.87$; squared cross validated correlation coefficient $R^2_{cv} = 0.80$; Fisher criterion $F = 39.08$; squared standard deviation $s^2 = 0.18$. **Table 5** presents the observed and predicted $log(1/EC_{50})$ values using Eq.3 together with descriptor values and eNP sizes.

[4] Pathakoti, K. *et. al. J. Photochem. Photobiol. B* **2014,** *130,* 234-240.

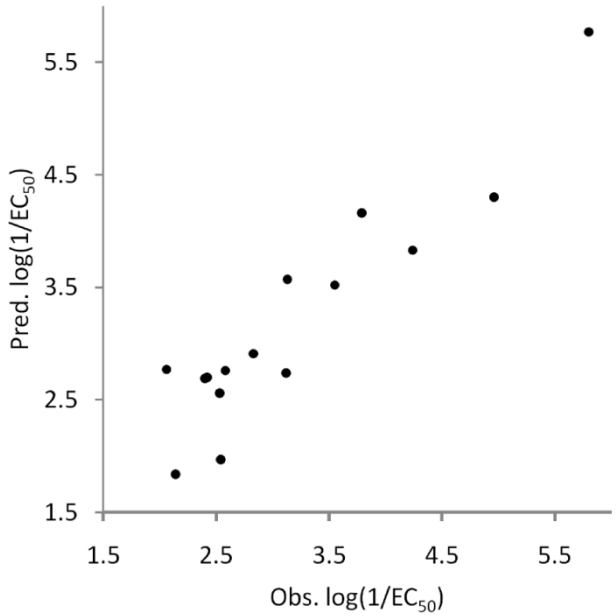


**Figure 12.** Plot of observed *vs*. predicted *log(1/EC$_{50}$)* values of metal oxide nanoparticles

Using the same approach, another QNAR model was constructed using data (**Table 6**) taken form Puzyn et al.(2011).

**Table 6** Experimental and predicted log(1/EC$_{50}$) values of nanoparticles, calculated nanodescriptors (ND) and size information. ND$_1$ is the *Average potential energy of atoms in the shell region of the eNP* and ND$_2$ is *Average potential energy of oxygen atoms in the core region of the eNP*.

| | **log(1/EC$_{50}$)** | | **Nanodescriptors** | | **NP size** |
|---|---|---|---|---|---|
| **NP** | **Exp.** | **Pred.** | ***ND$_1$* (eV)** | ***ND$_2$* (eV)** | **Diameter (nm)** |
| ZnO | 3.45 | 3.38 | -19.36 | -19.70 | 21.0 |
| CuO | 3.20 | 3.34 | -21.25 | -21.60 | 48.0 |
| $V_2O_3$ | 3.14 | 2.72 | -28.60 | -19.47 | 20.0 |
| $Y_2O_3$ | 2.87 | 2.75 | -27.19 | -18.00 | 32.7 |
| $Bi_2O_3$ | 2.82 | 3.01 | -17.04 | -8.36 | 51.0 |
| $In_2O_3$ | 2.81 | 2.75 | -27.88 | -18.94 | 59.6 |
| $Sb_2O_3$ | 2.64 | 2.74 | -28.04 | -18.97 | 20.0 |
| $Al_2O_3$ | 2.49 | 2.49 | -32.79 | -20.80 | 31.0 |
| $Fe_2O_3$ | 2.29 | 2.71 | -29.64 | -20.71 | 20.0 |
| $SiO_2$ | 2.20 | 1.96 | -41.98 | -23.11 | 20.0 |
| $ZrO_2$ | 2.15 | 2.22 | -32.16 | -14.06 | 25.0 |
| $SnO_2$ | 2.01 | 2.11 | -37.23 | -19.27 | 21.0 |
| $TiO_2$ | 1.74 | 1.77 | -43.31 | -21.05 | 15.0 |
| CoO | 3.51 | 3.37 | -19.83 | -20.14 | 20.0 |
| NiO | 3.45 | 3.37 | -19.92 | -20.33 | 20.0 |
| $Cr_2O_3$ | 2.51 | 2.68 | -30.37 | -21.09 | 20.0 |
| $La_2O_3$ | 2.87 | 2.77 | -12.12 | 4.24 | 24.6 |

Using the information in **Table 6** and the size-dependent nanodescriptors, a two parameter multilinear QNAR was developed:

$$\log\left({}^{1}/_{EC_{50}}\right) = 3.82 + 0.07ND_1 - 0.05ND_2 \qquad (4)$$

Where $ND_1$ in **eq 4** corresponds to the nanodescriptor *Average potential energy of atoms in the shell region of the nanoparticle* in electron volts, and $ND_2$ is the nanodescriptors corresponding to the *Average potential energy of oxygen atoms in the core region of the nanoparticle* in electron volts. The QNAR shows acceptable statistics for performance and stability:

$$\begin{cases} R^2 = 0.87 \\ R^2_{cv} = 0.81 \\ F = 45.26 \\ s^2 = 0.04 \end{cases}$$

**Figure 13** shows a plot of the experimental versus predicted endpoint values.

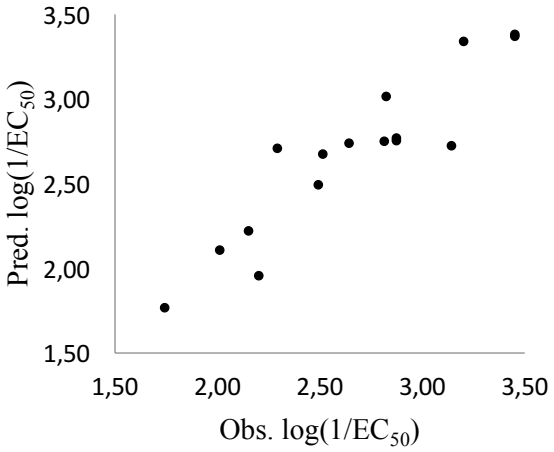


**Fig. 13** Plot of observed vs. predicted log(1/$EC_{50}$) values of nanosized metal oxides, based on the two nanodescriptor model (Eq. 4).

**Model interpretation.** The first nanodescriptor - $ND_1$ - in equation 4 is a very obvious choice, since many of the outstanding characteristics of eNPs are related to the uncompensated potential energies of the atoms at or near the surface of the particle. The descriptor is not that much composition dependent, instead it relates to the shape and size of the particle. The second nanodescriptor - $ND_2$ - is more composition specific, as the potential energy of the oxygen atoms in the unperturbed lattice of an oxide depend both on the lattice structure and the metal atom involved. Therefore, with just two descriptors the model can account for the chemical composition, the lattice structure, the size, and the shape of eNPs.

The computational method described above was designed to be expandable to allow the development of a more accurate representation of nanoparticles and more complex descriptors. While at the moment the descriptors were calculated from single-point energies, it is easily expandable to include full or partial minimization of the geometry of the nanoparticle before the calculation of descriptors or even perform molecular dynamics simulation of these systems to replicate the pyrolysis conditions used in the synthesis of nanoparticles. In this way, even the synthesis conditions can be included in the model facilitating their used for safe-by-design and for the optimization of nanoparticle's properties. Computationally more expensive potential improvements include the use of solvent and coating materials around the nanoparticle. In order to prove the benefits of such more elaborate approaches, however, a very consistent and accurate experimental dataset has to be used with known and controlled particle size distribution and other

variables. The successful modelling of the two nanoparticle toxicity datasets confirmed the potential of the newly-developed nanodescriptors.

**Objective: Establishment of a data mining framework and basic categorization criteria for the identification of nanoparticle categories (WP3).**

The large number of nanotechnology enabled products and the multitude of different types of nanomaterials makes impracticable, in terms of time and costs, their exhaustive hazard and risk assessment. Nanomaterial categorization criteria are needed to develop "grouping schemes" that will make nanosafety assessment more efficient. From a computational nanotoxicity perspective, the large number of possible nanoparticle types (e.g., diverse combinations of core composition, surface modifications and functionalizations) hinders the development of "universal" models. It is thus fundamental to develop similarity metrics involving different nanomaterial characteristics (e.g., nanostructure descriptors, physicochemical property profile and biological activity) across their entire life cycle. The use of appropriate similarity metrics will facilitate the grouping of nanoparticles into homogeneous categories where more accurate and reliable models can be developed and validated. The establishment of eNP categories will also enable the ranking of their environmental and human health impact paving the way to the development of a risk assessment framework for nanomaterials.
Within MODERN, different techniques and algorithms have been used to group the metal and metal oxide nanoparticles into similar groups using different types of information. The different category schemes developed in the current analysis are discussed in terms of the *soluble*, *active* and *passive* groups proposed by Arts et al., 2015 in their *DF4nanoGrouping* framework. In what follows, a given eNP is considered as *active* if it has $EC_{50}$ values lower than 100 mg/L for at least one of the tested species.
The data set in **Table 6**, covering material characters and hazard estimates for nanoparticles in MODERN's library have been used to illustrate the application of the hierarchical analysis.

**Table 6.** Toxicities of nanoparticle (eNP) suspensions to algae *Pseudokirchneriella subcapitata*, protozoa *Tetrahymena thermophila* and bacteria *Vibrio fischeri*.

| eNP | Algae $EC_{50}$ | Protozoa $EC_{50}$ | Bacteria $EC_{50}$ | BET Size (BET) | Hydrodinamic size (nm, DI water) | Zeta Potential (mV, DI water) | Oxidation level |
|---|---|---|---|---|---|---|---|
| ZnO | 0.1 | 1.84 | 11.52 | 20.4 | 171 | 16.4 | 2 |
| CuO | 0.43 | 2 | 1.78 | 13.1 | 130 | 17 | 2 |
| $TiO_2$ | 1.26 | 52.6 | 100 | 12.2 | 171 | -13.6 | 4 |
| $Fe_3O_4$ | 1.93 | 26.03 | 100 | 9.7 | 128 | 22.2 | 2.67 |
| $Co_3O_4$ | 1.11 | 100 | 100 | 11.5 | 99 | 23 | 2.67 |
| $Mn_3O_4$ | 1.34 | 100 | 100 | 15.2 | 395 | -14.4 | 2.67 |
| Pd | 0.41 | 100 | 55.42 | 15.1 | 127 | -27.8 | 0 |
| $SiO_2$ | 35.58 | 100 | 100 | 7.8 | 148 | -33.2 | 4 |
| $Al2O_3$ | 30.8 | 100 | 100 | 11.4 | 95 | 39.2 | 3 |
| $WO_3$ | 57.8 | 100 | 87.07 | 10.6 | 63 | -45.2 | 6 |
| MgO | 100 | 100 | 100 | 13.6 | 1964 | 6.9 | 2 |
| $Sb_2O_3$ | 100 | 100 | 73.74 | 20.5 | 125 | -24.3 | 3 |

**Categories derived from nanodescriptors. Figure 14** depicts the most significant groupings of nanoparticles obtained using a bootstrapped hierarchical clustering algorithm. Grouping was generated by using only information related to nanoparticles' structure through the complete set of 35 size-dependent nanodescriptors developed in WP1. Consistent groupings are obtained after changing nanoparticle's primary sizes from 5 nm to 30 nm. The analysis of the toxicity data for a set of 24 eNPs extracted from literature shows that the grouping, based solely on structural information, is unable to capture the toxicity of the eNPs. *Active* nanoparticles showing significant *in vitro* toxicity to BEAS-2B and RAW 264.7 cell lines are grouped together with *passive* eNPs (i.e., not triggering relevant cytotoxic responses). For instance, the group formed by {ZnO, CuO, NiO, CoO, MgO} includes both *active* and *passive* eNPs. A closer look at the fine structure of the

categories, reveals that the most soluble eNPs (i.e., ZnO, CuO), which are also know to share a toxicity mechanism driven by solubility and ion shedding are grouped together. The high structural similarity of these nanoparticles, that has a parallel in some of their physicochemical properties (e.g., solubility) as well as in their bioactivity profile can be subsequently used for model development and nano read-across.

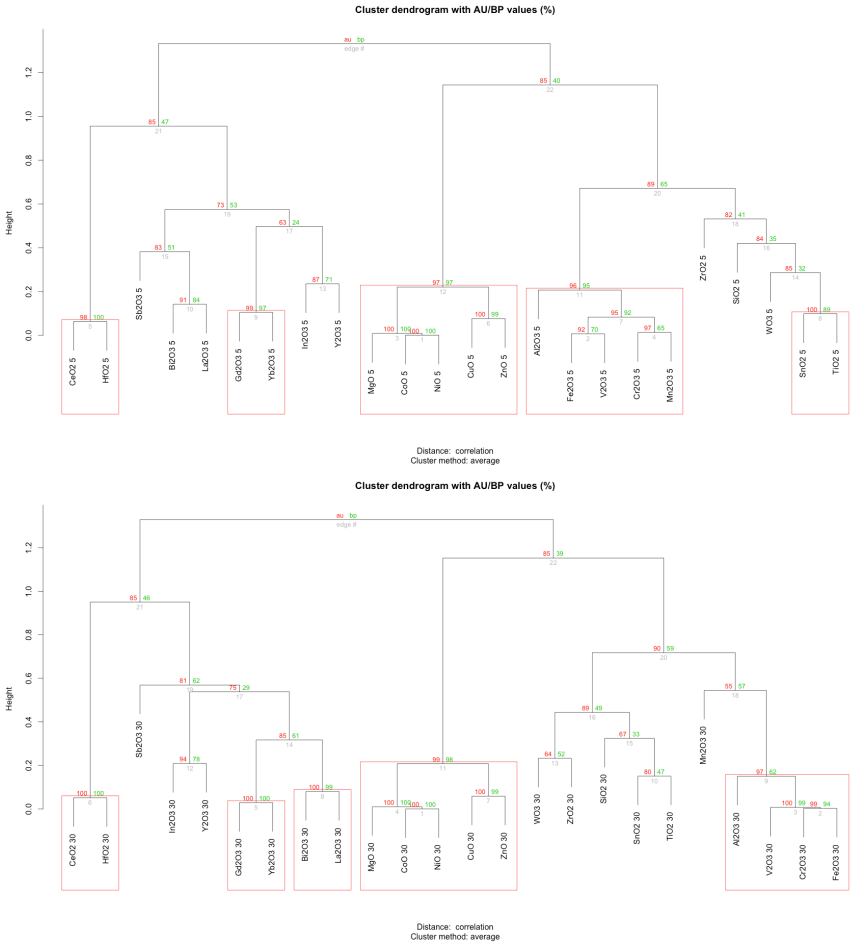


**Figure 14.** Hierarchical clustering of a library of 24 metal oxide (MeO) nanoparticles based on the size-dependent descriptors developed using molecular modeling. Clusters identified with high confidence (i.e., with p-values ≥ 95) after a multiscale bootstrap sampling process with 10 different sizes and 1000 replicates for each size are indicated by rectangles. (Top) Groups for spherical MeO nanoparticles of 5 nm. (Bottom) Groups for spherical MeO nanoparticles of 30 nm.

**Categories derived from physicochemical properties.** Categories can be developed from measured physicochemical properties of the eNPs. **Figure 15** depicts the categories obtained using the Self-Organizing Map (SOM) algorithm to group the 11 metal oxide nanoparticles in MODERN's library. Each SOM map unit ((i.e., circles in **Figure 15**) can be interpreted as a cluster. Accordingly, nanoparticles assigned to the same unit form a category. The features used for grouping included BET size, hydrodynamic diameter in DI water, zeta potential in DI water and the oxidation level (see **Table 6**). Prior to SOM development, data were centered and scaled. Map topology was defined as toroidal (i.e., periodic boundaries) to avoid border effects and the map grid was rectangular with a dimension of 3x2 units. The position of eNPs within each unit reflects their similarity (i.e., the closer the labels the more similar the eNPs). In addition, the distance of a nanoparticle to the unit center (i.e., center of each circle) is related to the ability of a given nanoparticle to act as a representative element for the group of eNPs assigned to the unit. The SOM analysis identifies 6 different groups of nanoparticles.

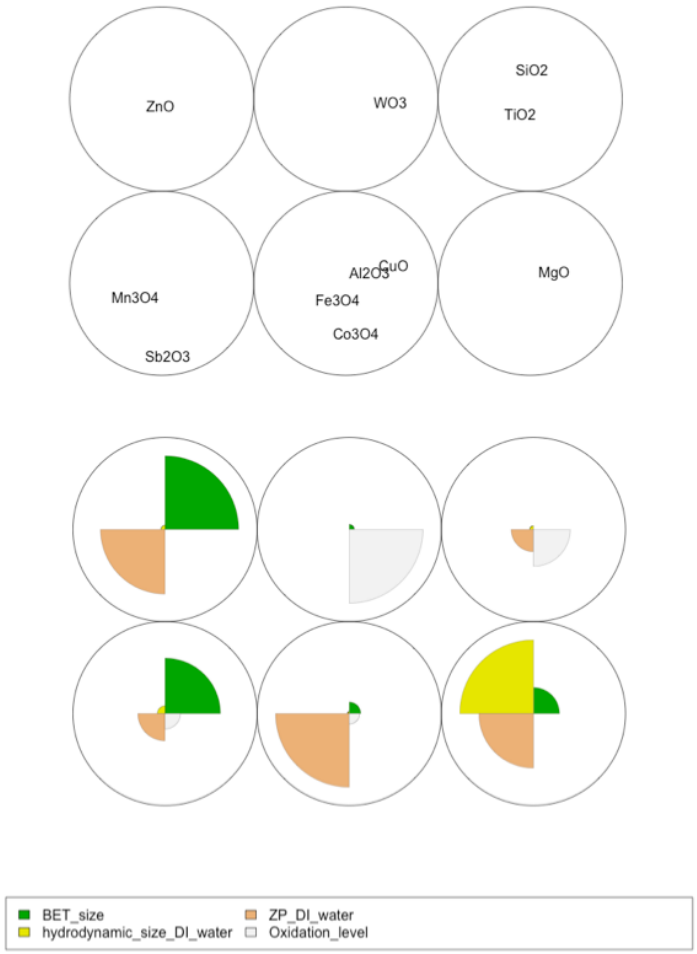


**Figure 15.** Self-Organizing Map (SOM) clustering of metal oxide nanoparticles in MODERN's library. Clustering was performed based on the group of physicochemical properties reported in Table 6. (Top) Identification of eNPs in each category. (Bottom) Physicochemical property profile of each category

Data in **Figure 15** provides the basis for the interpretation of the categories obtained from SOM analysis. Category 1 is formed only by ZnO and its main characteristics are large BET size and a moderate positive ZP in DI water. The distinctive features of Category 2 {$WO_3$} are the oxidation level and a highly negative surface charge. Category 3 comprises {$SiO_2$, $TiO_2$}, the main characteristics of this group are the oxidation level and negative surface charge. The representative eNP of this category is $TiO_2$. The fourth category includes {$Mn_3O_4$, $Sb_2O_3$} and its main features are similar to category 1. However, BET sizes are smaller and the surface charge in DI water is negative. The representative eNP of this category is $Mn_3O_4$. Category 5 is the most populated {CuO, $Al_2O_3$, $Fe_3O_4$, $Co_3O_4$} and contains positively charged eNPs. The category representative is $Fe_3O_4$. Finally, category 6 is formed by MgO and its distinctive property is the hydrodynamic size with large values. Categories 1, 2, 3 and 5 include eNPs which are either *soluble* or *active* to the species tested ($EC_{50}$ < 100 mg/L). Category 6 includes a *passive* eNP whereas category 4 mixes *active* with *passive* eNPs.

**Categories derived from the ecotoxicity profile.** Using a data-driven grouping approach based on community detection on complex networks three categories of eNPs were automatically detected. Complex networks are graphs containing a set of nodes, representing nanoparticles, and a set of edges connecting pairs of nodes. The grouping of nanoparticles inside the network was done looking for what it is called the analysis of the community structure of the networks, i.e. a partition of the network into communities, which are subsets of nodes more strongly connected between them than with the rest of the nodes in the network.

Interestingly, the category that contains *soluble* and *active* eNPs, formed by {ZnO, CuO, $Fe_3O_4$ and $TiO_2$}, is consistent with the grouping observed in the trend analysis of electronic structure descriptors (**Figure 10**). The second category that comprises {$Mn_3O_4$, $Co_3O_4$, $SiO_2$, and $Al_2O_3$ also corresponds to *active* eNPs. Finally, the third category that includes {$WO_3$, MgO and $Sb_2O_3$} corresponds to eNPs which are *passive* from the ecotoxicity viewpoint (i.e., $EC_{50}$ > 100 mg/L for at least two species).

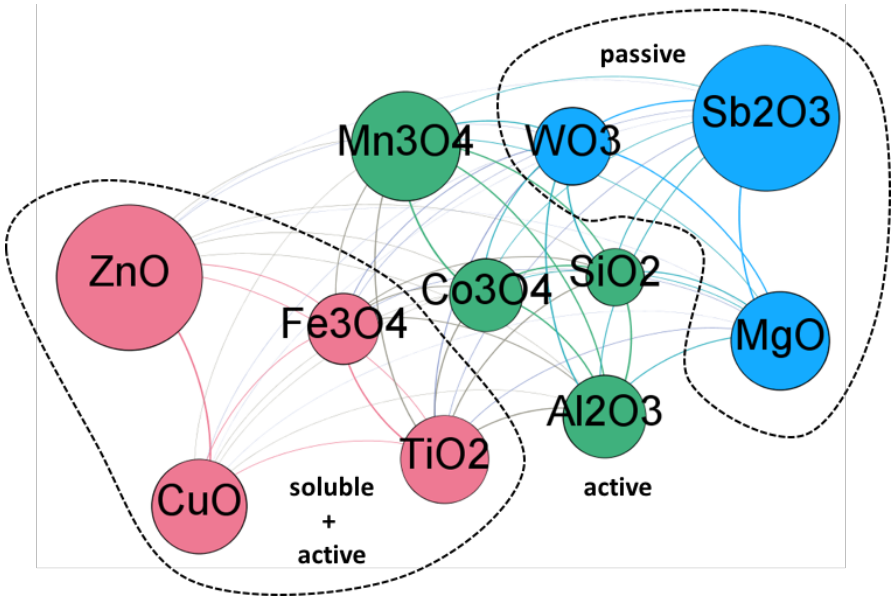


**Figure 16.** Categories identified from the integrated (algae + protozoa + bacteria) ecotoxicity profile. Color codes correspond to different eNP categories

**Categories identified from integrated structure-physicochemical and ecotoxicological data.** Relevant eNP categories can be identified from data by integrating heterogeneous information related to multiple aspects of the nanomaterial. **Figure 17** depicts the categories identified using complex network analysis after integrating three different types of information including structure, physicochemical properties and ecotoxicity. The *soluble* category includes ZnO and CuO whose toxicity is driven by solubility. The category corresponding to the *active* nanoparticles is formed by three subgroups with different activity levels and includes $Fe_3O_4$, $TiO_2$, $Mn_3O_4$, $Co_3O_4$, $SiO_2$, $Al_2O_3$ and $WO_3$. Finally, the *passive* category is formed by $Sb_2O_3$ and MgO.

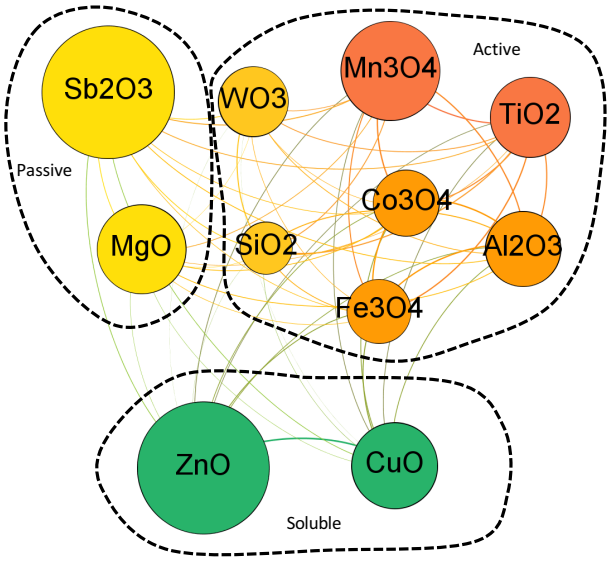


**Figure 17.** Grouping obtained using complex network analysis techniques. Data used for grouping includes size-dependent nanodescriptors, physicochemical properties (BET size, ZP in DI water, oxidation state) and ecotoxicity profile for algae, bacteria and protozoa. The size of each node is proportional to nanoparticle's BET size. Colors correspond to communities (groups) of eNPs identified using modularity.

**Objective: Development of a hazard ranking scheme suitable to rank eNPs and their categories according to their potential environmental and human health impact.**

What is missing is a robust regime, where the present knowledge on nanomaterial (NM) characteristics and hazard information can lead to robust decisions in relation to risks. The decisions should preferably be based on a regime involving comprehensive models that implement simple and logical algorithms, as this will ensure a robust frame with a wide distribution and fast implementation to many stakeholders. The foundation for such tools has been developed within MODERN.

In MODERN, a framework which makes use of the molecular descriptors and toxicological profiling of engineered Nanoparticles (eNPs) was developed. The development and implementation focused on (i) a robust hazard ranking scheme suitable to prioritise and rank eNPs and (ii) a more detailed data mining framework that is suitable to identify similarity in eNP patterns according to their potential environmental and human health impact. To develop this, the central information on eNPs Environmental, Health and Safety (EHS) related descriptors has been identified and evaluated. This includes the identification of physicochemical descriptors that identify the eNPs (e.g. size, surface area) and related biological descriptors (e.g. effect concentrations for cell viability).

Hence, MODERN developed ranking models that enabled risk regulators to have a robust tool for prioritising, ranking and reading across information between materials. The tool was based on ordering techniques that imply that the results are robust and consistent, even if more complex models are applied based on the same information. The conclusions drawn from this tool do not adopt the added uncertainty coming from the task of aggregating several parameters to form one single ranking value based on non-validated weighing factors or relationships. Hence, the tool can be the first and robust steps in risk evaluation of eNP. It was shown how hazard data from different species could be ranked together using a dataset developed within MODERN that consists of 12 different nanomaterials with toxicity data for three aquatic species (*in vivo*) and three cell types (*in vitro*). Further, it was possible to identify when major differences in toxicity between species occurred. This ranking could be combined and correlated to ranking based on physical-chemical parameters. In this way, it was possible to show the rank of nanomaterial versus the toxicity values for different species and to identify the material characteristics that best

correlated with the toxicity values. Similar calculations were performed with datasets obtained from the literature. It was further discussed how to deal with missing information and how possible classification schemes and risk banding regimes could be identified.
In MODERN, more comprehensive tools were developed based on e.g. step-wise regression, principal component analysis, and self-organising maps. The latter techniques, compared to the prior ranking tools, are not able to handle categorical data, but can include quantified distance, complex distributions and, hence, more information. These sophisticated data-mining techniques, such as the Self-Organizing Map or algorithms to generate Association Rules combined with feature selection methods, provided an adequate framework for knowledge extraction from nanosafety datasets. These techniques were enhanced by automatic category interpretation via ontology-based inference and expert validation, which provided the required science based criteria for grouping of eNPs. It was shown from both literature and MODERN's generated data how the nanomaterials could be grouped based on their physical-chemical parameters.
In summary, it is here outlined how various techniques can be used for risk assessment with focus on decision making in regard to read across. The hazard ranking approaches developed in MODERN may further support a priori or posterior group of the materials and in this way optimize the risk characterization.

# POTENTIAL IMPACT

MODERN outcomes will contribute to the assessment of eNP effects and to the reduction of animal testing by facilitating the development of methods for inferring toxicity of eNP via the integration of *in vivo*/*in vitro* studies and *in silico* models. These two elements will serve in the long-term as the basic building blocks of a predictive framework that will guide the production of new safe-by-design eNPs. In what follows, the potential impact of MODERN is presented in the context of each RTD work-package.

**WP1: Physicochemical, molecular and structural properties of eNPs**
MODERN has established a novel understanding regarding chemical and/or biological mechanisms governing eNP impact. The project developments will trigger new research opportunities and increase awareness regarding the safe use of nanoproducts (safe-by-design strategies). Using FSP, a library of ultrafine, single crystalline metal and metal oxide eNPs has been synthesized and fully characterized. Data generated within MODERN will be available to the Nanosafety Community from the nanoDMS system. In fact the data management system is in itself a significant outcome of the project since it implements the first ISA-TAB-Nano compliant database for nanosafety data.
The computational characterization of the molecular structure and physicochemical properties of eNPs carried out in WP1 will impact at two different levels. First, MODERN has developed new nanodescriptors suitable to describe the structure of eNPs from the viewpoint of their electronic structure as well as from the view point of their size effects. The main importance of these scientific results lies in breaking the barrier of the description of nanoparticles. From the former chemical composition or small fragment based approach to the description of full particles, including their shape and size. For the first time, it is possible to build nanoparticle – activity models that reflect the true character of nanoparticles, without making specific assumptions on the source data that is being modelled, in particular the size distribution (or lack thereof). This conceptual improvement not only allows the creation of better performing quantitative models, but brings new options to the general understanding and ways of analysis of nanoparticle properties or characteristics.

**WP2: *In silico* profiling of the environmental and health impact of eNPs**
MODERN has also contributed to the establishment of new QNARs from the nanodescriptors developed in WP1. The analysis of the eNP properties obtained and characterized in WP1 together with the biological activity profiles determined in WP2 has contributed to identify data gaps and has the potential to be subsequently used as a diagnostic and design tool to respectively trigger/drive new experimental characterization work for safe-by-design nanomaterials. MODERN will facilitate open access to the rich dataset of ecotoxicity data for three species (algae, protozoa and bacteria) exposed to the eNPs in MODERN's library. These data will also be useful to validate and extend current nanotoxicology models. In summary, the data-driven approach for the *in silico* characterization of the effects produced by eNPs on biological systems (aquatic and terrestrial ecosystems) developed in MODERN will impact the nanosafety community since the statistical analysis and mining of these data will provide the basis for *in silico* profiling of mechanisms of action and for the establishment of more advanced quantitative nano structure-activity relationships describing the biological activity and the toxicity behavior of eNPs in the human body and in the environment.

**WP3: Identification of eNP categories and basic hazard ranking**
The eNP signatures, obtained from the information collected/generated in WP1 and WP2, have served to identify similarities in the structural, molecular, physicochemical property profiles, and biological activity for categorizing nanoparticles and establishing relations between experimental and calculated properties. Both the *in silico* models and the categorization methodology will contribute to advance towards the design of integrated testing strategies (ITS) for nanomaterials suitable for regulatory purposes. The contribution of MODERN's research to the development of

an ITS scheme for eNPs will provide the framework and technical basis to fulfill safety levels and animal welfare goals, while being practicable from a technical and an economic perspective. Specifically, the in silico models developed in MODERN will contribute to the ethical goal of animal welfare facilitating the replacement, reduction and refinement of animal testing, in accordance with general public and societal needs and as laid down in Directive 86/609/EEC on the Protection of Laboratory Animals.
Regarding hazard ranking and risk assessment, decisions should preferably be based on comprehensive models implemented into simple and logic algorithms since this will ensure a wide distribution and the fast implementation to many stakeholders. The foundation for such tools has been developed within MODERN. Hence, the impact of the methodologies and tools developed in MODERN is at least two-fold, (i) the MODERN model progresses the scientific basis for read across models, which enable the identification of eNP descriptors that correspond to certain toxic effects. The other impact is the applied side, i.e. the industrial and regulatory aspect, where the developed framework allows industrial (i) material developers to construct safer by design materials. Our framework for risk assessment also allows regulators to (i) model, rank and prioritize the available information and, hence, pinpoint where more research is needed, and (ii) to identify risk banding tools and potential groups of toxic nanomaterials. These modelling, prioritization, ranking and grouping approaches are fully in line with regulatory initiatives, where robust grouping and ranking (based on inclusion of comprehensive information) paradigms are requested. This is similar to ongoing initiatives for prioritization of chemicals.

**Impact on the nanosafety community**
The identification of eNP categories and the development of the basic hazard ranking scheme developed in WP3 will represent a step towards the promised eNPs safety for success. MODERN has generated information and computational methods relevant for the understanding on nano-bio interactions in cells (*in vitro*), and terrestrial and aquatic species (*in vivo*). The knowledge on nano-bio- interactions obtained will serve to further refine eNP categories and to explain their mechanisms of toxicity. Accordingly, MODERN has contributed to the implementation of the EC Action Plan for Nanotechnology by (i) generating and collecting nanosafety-relevant data; (ii) developing novel QNAR models suitable to support regulatory demands; (iii) providing new information to support the mechanistic interpretation of toxicity effects across relevant species for ecotoxicity studies; (iv) creating new protocols for eNPs categorization and hazard ranking; (v) promoting the safe-by-design development and production of products from nanotechnology; and (vii) contributing to the development of new guidelines for the sustainable and responsible development of nanotechnologies.

**European dimension and social awareness**
The activities carried out by MODERN Consortium members have contributed to the reinforcement of the international dimension of European research and collaboration between industry, researchers, environmental agencies, authorities (at Member State and European level) and international standardization bodies. The hazard ranking and risk assessment strategy developed in MODERN will contribute to support governance in nanotechnology by facilitating informed decision-making to EU regulatory bodies, agencies and authorities. Policies could, thus, be established to safeguard consumers while taking full advantage of the advancements that the new generation of safe nanomaterials will bring to the economy and competitiveness of EU industry. In this context, MODERN outcomes will contribute to secure the responsible development of nanotechnologies and to assist public engagement on discussing their risks. Thus, it will help establishing sound social awareness on the benefits that eNPs have in daily use consumer products. Given the leading role that Europe has to maintain in the future worldwide market underpinned by nanotechnology, the results of the project have the potential to contribute to the necessary acceleration of the commercialization of the new generation of nanomaterials via safe-by-design strategies. The sound collaboration with the other modeling projects funded in the NMP.2012.1.3-2 has also reinforced the European dimension of the project.

In summary, both the novel nanodescriptors and the new and improved models enable to bring the understanding of the nanoparticle world out from the scientific community and research facilities and closer to the average citizen, thus potentially avoiding uninformed reactions of the public in either direction to anything considered as "nano", as we have seen to happen in recent years. The improved understanding of the benefits of nanoparticles should allow new businesses and products to emerge, boosting economy. The improvement of the quality of materials and products due to the superior properties of nanomaterials is expected to be also accompanied by both reduced costs as well as reduced impact to the environment, as less bulk material is required for obtaining the same target properties.

Improved understanding of the safety issues of nanomaterials should have twofold impact. First, a more knowledgeable public will be less accepting to poor practices of material handling and safety by the producers. Also producers of various nanomaterials would have an improved understanding of both the beneficial characteristics of their potential products but also the hazards at workplace and requirements for material handling. Regulators would have new and improved tools for assessing the safety of nanomaterials. Last, but not least, a knowledgeable public would be less likely to fall for any mass campaigns, either for or against the use of nanomaterials without analyzing the benefits and risks related to the real exposure scenarios in each particular case.

In conclusion, the overall expected impact of MODERN is the progress in understanding and describing the properties of nanomaterials, at scientific, production, regulatory and general public levels.

## References


1. Marchese Robinson, R. L., Cronin, M. T. D., Richarz, A.-N. & Rallo, R. An ISA-TAB-Nano based data collection framework to support data-driven modelling of nanotoxicology. *Beilstein J. Nanotechnol.* **6,** 1978–99 (2015).
2. Nel, A. *et al.* Understanding biophysicochemical interactions at the nano–bio interface. *Nat. Mater.* **8,** 543–557 (2009).
3. Krug, H. F. & Wick, P. Nanotoxicology: an interdisciplinary challenge. *Angew. Chem. Int. Ed. Engl.* **50,** 1260–78 (2011).
4. Neese, F. The ORCA program system. *Wiley Interdiscip. Rev. Comput. Mol. Sci.* **2,** 73–78 (2012).
5. Perdew, J. P., Burke, K. & Ernzerhof, M. Generalized Gradient Approximation Made Simple. *Phys. Rev. Lett.* **77,** 3865–3868 (1996).
6. Grimme, S., Antony, J., Ehrlich, S. & Krieg, H. A consistent and accurate ab initio parametrization of density functional dispersion correction (DFT-D) for the 94 elements H-Pu. *J. Chem. Phys.* **132,** 154104 (2010).
7. Weigend, F. & Ahlrichs, R. Balanced basis sets of split valence, triple zeta valence and quadruple zeta valence quality for H to Rn: Design and assessment of accuracy. *Phys. Chem. Chem. Phys.* **7,** 3297–305 (2005).
8. Puzyn, T. *et al.* Using nano-QSAR to predict the cytotoxicity of metal oxide nanoparticles. *Nat. Nanotechnol.* **6,** 175–8 (2011).
9. Arts, J. H. E. *et al.* A decision-making framework for the grouping and testing of nanomaterials (DF4nanoGrouping). *Regul. Toxicol. Pharmacol.* **71,** S1–27 (2015).
10. Zhang, H. *et al.* Use of metal oxide nanoparticle band gap to develop a predictive paradigm for oxidative stress and acute pulmonary inflammation. *ACS Nano* **6,** 4349–68 (2012).
11. Liu, R. *et al.* Development of structure-activity relationship for metal oxide nanoparticles. *Nanoscale* **5,** 5644–53 (2013).